AD-A234 731

REPORT DOCUMENTATION PAGE

1a. REPORT SECURITY CLASSIFICATION: UNCLASSIFIED	1b. RESTRICTIVE MARKINGS
2a. SECURITY CLASSIFICATION AUTHORITY	3. DISTRIBUTION/AVAILABILITY OF REPORT: Approved for public release; distribution unlimited.
2b. DECLASSIFICATION/DOWNGRADING SCHEDULE	
4. PERFORMING ORGANIZATION REPORT NUMBER(S)	5. MONITORING ORGANIZATION REPORT NUMBER(S): AFOSR-TR-88-1191
6a. NAME OF PERFORMING ORGANIZATION: Univ of Massachusetts; 6b. OFFICE SYMBOL (If applicable)	7a. NAME OF MONITORING ORGANIZATION: AFOSR/NE
6c. ADDRESS (City, State and ZIP Code): Amherst MA 01003	7b. ADDRESS (City, State and ZIP Code): Bldg 410, Bolling AFB DC 20332-6448
8a. NAME OF FUNDING/SPONSORING ORGANIZATION: AFOSR/NE; 8b. OFFICE SYMBOL (If applicable): NE	9. PROCUREMENT INSTRUMENT IDENTIFICATION NUMBER: AFOSR-84-0377
8c. ADDRESS (City, State and ZIP Code): Bldg 410, Bolling AFB DC 20332-6448	10. SOURCE OF FUNDING NOS. — PROGRAM ELEMENT NO.: 61102F; PROJECT NO.: 2301; TASK NO.: A1; WORK UNIT NO.:
11. TITLE (Include Security Classification): Optical Generation of Millimeter Waves	
12. PERSONAL AUTHOR(S): Dr De Fonzo	
13a. TYPE OF REPORT: Final; 13b. TIME COVERED: FROM 01Oct84 TO 30Sep 87	14. DATE OF REPORT (Yr., Mo., Day):	15. PAGE COUNT:
16. SUPPLEMENTARY NOTATION	
17. COSATI CODES — FIELD / GROUP / SUB. GR.	18. SUBJECT TERMS (Continue on reverse if necessary and identify by block number)

19. ABSTRACT (Continue on reverse if necessary and identify by block number)

During the last year of the grant we began developing theoretical techniques for the analysis of the propagation and radiation properties of the device structures we reported in Applied Physics Letters entitled "Optoelectronics Transmission and Reception of Ultrashort Electrical Pules". These structures are comprised of a complanar stripline coupled to a exponential tapered stripline antenna. We inititated the development of two models. One model describes the dispersion of coplanar striplines over a wide range of dimensions and frequencies. The model is full wave analysis in the spectral domain using Galerkins method.

20. DISTRIBUTION/AVAILABILITY OF ABSTRACT: UNCLASSIFIED/UNLIMITED ☐ SAME AS RPT ☐ OTIC USERS ☐	21. ABSTRACT SECURITY CLASSIFICATION: UNCLASSIFIED
22a. NAME OF RESPONSIBLE INDIVIDUAL: Schlossberg	22b. TELEPHONE NUMBER (Include Area Code): (202) 767-4908; 22c. OFFICE SYMBOL: NE

DD FORM 1473, 83 APR — EDITION OF 1 JAN 73 IS OBSOLETE.

91 4 15 055

DISCLAIMER NOTICE

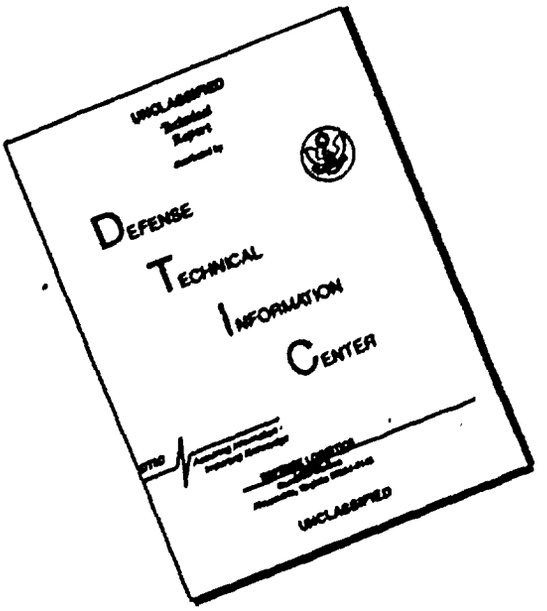

THIS DOCUMENT IS BEST QUALITY AVAILABLE. THE COPY FURNISHED TO DTIC CONTAINED A SIGNIFICANT NUMBER OF PAGES WHICH DO NOT REPRODUCE LEGIBLY.

Accepted for Pub. -
Picosecond elect. + optoelect.
Springer Verlag.
Electrophysics series
(to be pub)

Picosecond Optoelectronic Transceivers

Alfred P. DeFonzo, Charles R. Lutz and Madhuri Jarwala
Department of Electrical and Computer Engineering
The University of Massachusetts, Amherst, MA 01003

Accession For
NTIS
DTIC
U.
J...
By
A-1

1. Abstract

Picosecond photoconductivity is used to generate and sense transient millimeter wave radiation from monolithic broadband tapered slotline antennas integrated on ion damaged silicon on sapphire substrates. The far field is observed to consist of a traveling wave component and a standing wave component. The time dependent electromagnetic impulse response of these optoelectronic transceivers is also modeled.

2. Introduction

Recent studies have demonstrated that picosecond photoconductivity can be used to generate electromagnetic transients of picosecond duration [1]. The use of photoconductivity to generate millimeter wave radiation is a relatively new concept in picosecond electronics. It has many practical and spectroscopic applications, including developing a new class of devices capable of generating, controlling, and detecting millimeter waves. Investigations of such transients from discontinuities in microstrip lines [2] deposited on semiconductor substrates indicate the potential for producing intense coherent pulses with durations less than one picosecond, however, the structures used in these previous experiments were not optimized for efficient radiation of the resulting transient. To provide some control of the spatial and temporal distributions of the photoconductively generated radiation, more sophisticated antenna elements must be employed.

We present the results of a study of the picosecond impulse response of photoconductively driven integrated microelectronic transmitter and receiver antennas fabricated on a common semiconductor substrate. In addition further experiments were conducted in which an intervening air gap separated the transmitting and receiving antennas. The advantages of this method can be summarized as follows: Unlike the transmission line gaps of the past [1,3], our antennas are designed for radiation of picosecond transients. We have incorporated a pump/probe sampling technique in the design of the experiment, hence our measurements will be more accurate and we expect to observe high frequency components. The photoconducting gap driving the antenna is an integral part of the antenna structure and there is no aperture between transmitter and receiver. Thus, these structures are completely planar and can be easily fabricated on semiconductor substrates using conventional photolithographic techniques. Also. the antennas are small in size and are consequently compatible with other integrated millimeter wave circuits.

3. Experimental Design

The principle of our experiments is illustrated in Fig. 1. Identical transmitting and receiving antennas are fabricated on silicon on sapphire (SOS) substrates. The dimensions of the antenna were obtained by scaling down the design of the Vivaldi aerial first proposed by Gibson [4]. The length l, height h, and aperture sizes a_1 and a_2 were as follows: l= 2.96mm, h=3.8mm, a_1=25um, a_2=1.9mm. The distance between generator and detector was 9mm and the separation between transmitting and receiving antennas when fabricated on the same substrate was 3mm. Two antenna shapes were investigated. One was an Exponentially Tapered Slot Antenna, ETSA. The other was a Linearly Tapered Slot Antenna, LTSA.

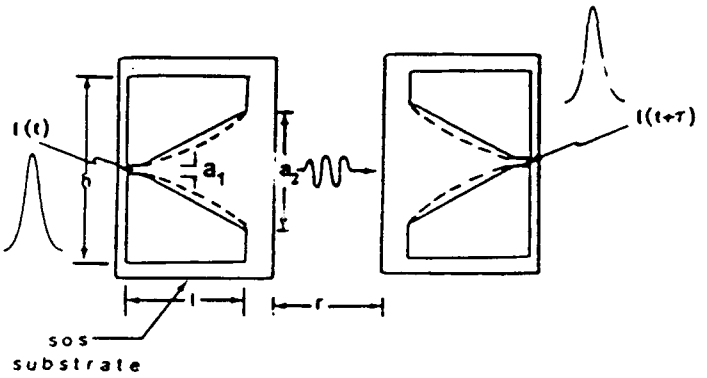

Fig. 1. Schematic of experimental configuration using matched optoelectronic antenna pairs. Dotted line indicates Exponentially Tapered Slot Antenna (ETSA). Solid line indicates Linearly Tapered Slot Antenna (LTSA).

The duration of the photoconductive transients is controlled by bombarding the silicon epilayer with energetic ions. In our experiments we bombarded the silicon with 100Kev and 200Kev O+ ions to a dosage of 10^{15} cm^{-2}. The antennas were fabricated on the radiation damaged substrates from aluminum films using standard photolithographic techniques. The photoconductive generator for the transmitting antenna is comprised of a short segment of slot line. This slot is DC biased and discharged photoconductively by illuminating the gap with a picosecond optical pulse. The discharge current pulse propagates into the antenna region where it dissipates radiatively. The radiated field which is emitted along the endfire direction of the antenna propagates to the opposing antenna. The received field results in transient bias voltage across the receiver slot line at a time equal to the propagation delay. This voltage is sampled photoconductively by illuminating the semiconductor material within the slot line with a second picosecond optical pulse derived from the same source as the exciting pulse and delayed by a variable time τ. The time dependence of the received signal is obtained by varying the time delay over the duration of the received transient.

4. Results. Transceivers on Common Substrate

In Fig. 2 we show a trace of the correlation for the ETSA pair. Superimposed is a direct correlation of the photoconductive transient measured on the same material using a conventional microstrip correlator [5]. The data clearly demonstrates that the signal received is the time derivative of the photoconducting driving pulse. Earlier work at much longer time scales [6] indicates that the ETSA takes the time derivative of the generator signal on transmission.

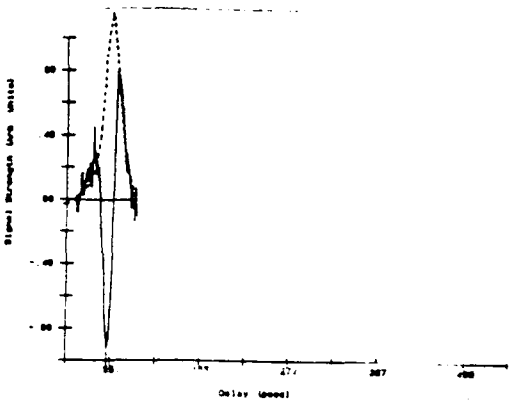

Fig. 2. Correlation trace of ETSA pairs on common subtrate showing isolated traveling wave component. Dotted line is the independently measured photoconductive pulse correlation.

5. Transceiver Pairs Separated by Air Gap

The measured correlation traces shown in Figs. 3(a) and 3(b) are the results obtained when the transmitting and receiving antennas were on different substrates separated by air gaps of approximately 1cm and 0.7cm respectively. Figure 3(a) is the signal obtained for the LTSA and Fig.3(b) is the result for an ETSA. The dashed curve in each figure corresponds to the correlation of the photoconductive driving pulse.

The results for the air spaced ETSA and LTSA are clearly different from those obtained for the same antennas fabricated on a common substrate. Each correlation trace indicates the presence of a fast transient followed by a decaying oscillation of much lower frequency. When the antennas are on the same substrate the oscillatory component is largely suppressed due to the guiding effects of the closely spaced ends of the antenna structure. The data can be accurately predicted using a model response function derived from antenna theory [7].

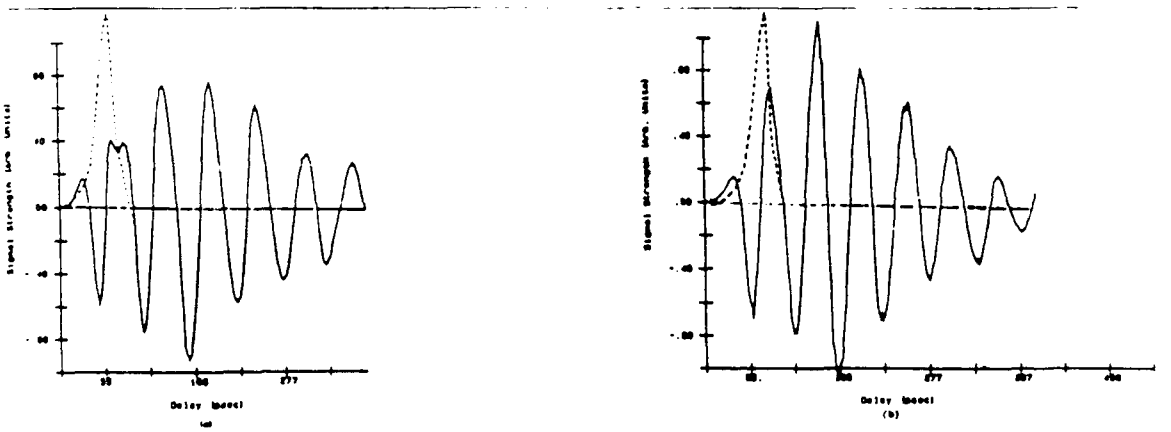

Fig. 3. Correlation traces with antennas on seperate substrates (a) LTSA (b) ETSA

6. Modeling of Transient Behavior

A model based on concepts found in the antenna literature has been developed which accurately predicts the picosecond photoconductive response of these structures. Two distinct radiation mechanisms operate in these devices - a travelling wave mechanism which produces the

initial transient and a standing wave mechanism which is associated with the longer time oscillatory radiation. The total measured response is the sum of the traveling wave response and the standing wave response delayed by the difference in propagation times in the antenna. The calculated response based on this model is shown in Fig. 4. Recent experiments have measured responses in which thesingle transient has been isolated from the standing wave component and is in fact the only signal radiated [8].

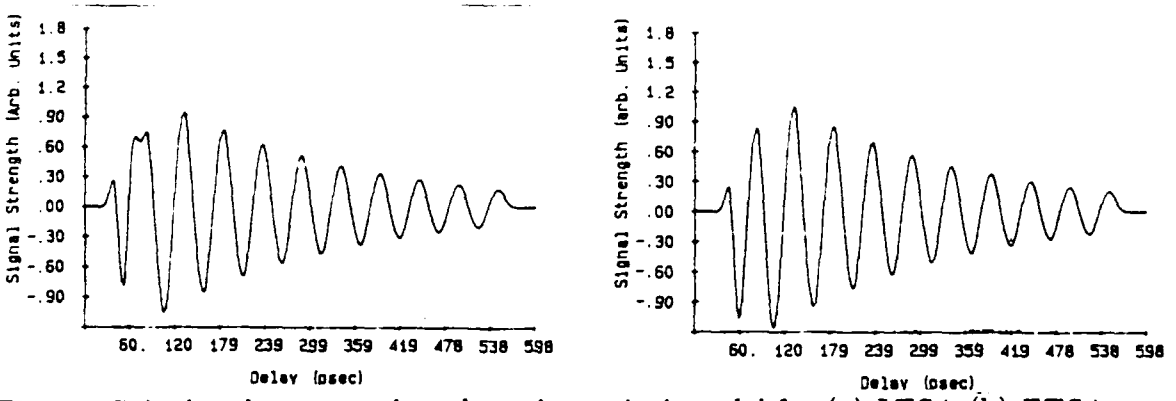

Fig. 4. Calculated response based on theoretical model for (a) LTSA (b) ETSA

7. Conclusions

We have shown that a new class of picosecond optoelectronic devices, fabricated using planar antenna technology, can be used to generate and sense millimeter have radiation. Our results indicate that these structures can be readily scaled down to the dimensions required for operation with femtosecond transients. In addition, a time domain model of the broadside transient radiation from these antennas has been proposed. The development of these devices will provide insights into a variety of transient electromagnetic problems of practical and fundamental interest. This work was directly supported by the Air Force Office of Scientific Research, (Grant AFOSR-84-0377). Additional support for our general efforts were provided by the National Science Foundation (Grant# NSFECS-8404495).

References

1. D.H. Auston, K.P. Cheung, and P.R. Smith, Appl. Phys. Lett., 45, 284, (1984).
2. J.R. Karin, P.M. Downey, and R.J. Martin, IEEE J. of Quantm. Electrns., QE-22, 677, (1986).
3. D.H. Auston, and P.R. Smith, Appl. Phys. Lett., 43, 631, (1983).
4. P.J. Gibson, Proc. 9th European Microwave Conference, Brighton, 101, (1979).
5. D.H. Auston, A.M. Johnson, P.R. Smith, and J.C. Bean, Appl. Phys. Lett., 37, 371, (1980).
6. R. Heidemann, Th. Pfeiffer, and D. Jager, Electrncs. Lett., 19, 316, (1983).
7. A.P. Defonzo, M. Jarwala, and C.R. Lutz, submitted IEEE/OSA Conference on Lasers and Electro-Optics, 1987.
8. A.P. Defonzo and C.R. Lutz to be published.

Accepted for pub.
Applied Phys. Ltrs.

TRANSIENT RESPONSE OF PLANAR INTEGRATED OPTOELECTRONIC ANTENNAS

Alfred P. DeFonzo, Madhuri Jarwala, and Charles Lutz

Department of Electrical and Computer Engineering
University of Massachusetts, Amherst, MA 01003
(413) 545-2374

Abstract: Broadband tapered slot antennas monolithically integrated on ion damaged silicon on sapphire substrates, are driven by picosecond photoconductivity to generate and detect millimeter waves. The time dependent electromagnetic impulse response of these tranceivers is modeled by relating the antenna structure and the shape of the exciting pulse. The far field response is observed to consist of a traveling wave component and a standing wave component, which is also predicted by the model.

1 Introduction

Picosecond photoconductive transients have recently been used to generate picosecond electromagnetic transient radiation [1]. Recent studies of such transients from discontinuities in microstrip lines [2] deposited on semiconductor subtrates indicate the potential for generating intense coherent pulses with durations less than one picosecond for practical and spectroscopic applications. Here, we demonstrate the concept of a new class of picosecond optoelectronics. We present the results of a study of the picosecond impulse response of photoconductively driven integrated microelectronic transmitter and receiver antennas. We also show how picosecond techniques improve our understanding of the behavior of linear antennas.

The principle of our experiments is illustrated in Figure 1. Identical transmitting and receiving antennas are fabricated on silicon on sapphire substrates. The photoconductive generator for the transmitting antenna is comprised of a short segment of aluminum slot line deposited over an ion implanted layer of silicon. The slot is dc biased and discharged photoconductively by illuminating the gap with a picosecond optical pulse. The discharge current pulse propagates into the antenna region where it dissipates radiatively. The radiated field which is emmitted along the endfire direction of the antenna propagates to the opposing antenna. The received field results in a transient bias voltage across the receiver slot at a time equal to the propagation delay. This voltage is sampled photoconductively by illuminating the semiconductor material within the slot with a picosecond optical pulse derived from the same source as the exciting pulse and delayed by a variable time τ. The time dependence of the received signal is obtained by varying the time delay over the duration of the received transient.

2 Experiment

The duration of the photoconductive transients is controlled by bombarding the silicon epilayer with energetic ions. In our experiments we bombarded the silicon with $100kev$ and $200kev$ 0+ ions to a dosage of $10^{15}cm^{-2}$. The antennas were fabricated on the radiation damaged substrates from aluminum films using standard photolithographic techniques. Two antenna shapes were investigated. One was an exponentially tapered slot antenna, ETSA, [3]. The other was a linearly tapered slot antenna, LTSA [3]. The overall length of the antennas was $2.9mm$, the width at the aperture was $1.9mm$ and the slot width was 30 microns.

The optical pulses were obtained from a modelocked dye laser in the standard three mirror configuration. Modelocking was achieved by synchronously pumping an R6G dye jet with the frequency doubled output of an actively modelocked Nd:YAG laser operating at $1.06microns$.The standard autocorrelation SHG measurement technique [4] was used to determine the pulse width of the modelocked dye laser pulses. The minimum pulse width was measured to be less than $2ps$ and could be lengthened to $6ps$ by adjusting the cavity parameters. The pulses were split using a variable delay line in the standard pump probe configuration. The pump pulse was focussed into the transmitter slot and the delayed probe pulse was focussed into the receiver slot. The transmitter slot was dc biased in the 10 to 40 volt range. The time sampled receiver signal was passed through a low frequency amplifier and plotted as a function of time delay between the pump and probe pulse on an $x - y$ plotter.

The measured correlation traces are show in Figure 2. Figures 2 (a) and (b) show the results obtained when the transmitting and receiving antennas were on different substrates separated by air gaps of approximately $1cm$ and $0.7cm$ respectively. Figure 2 (a) is the

result obtained for LTSA. Figure 2 (b) is the result obtained for an ETSA. Figure 2 (c) shows the result obtained for an ETSA transmitter receiver pair fabricated on common substrate with a separation distance of $3mm$. The dashed curve in each figure is the correlation trace independently obtained from a photoconductive cross correlator configuration commonly used to determine the duration of photoconductive transients [5].

The results for the air spaced ETSA and LTSA are similar. Each correlation trace indicates the presence of a fast transient followed by a decaying oscillation. When the antennas are on the same substrate the oscillatory component is largely suppressed. Direct comparison of the photoconductive correlation with the antenna correlation indicates that initial transient is the derivative of the photoconductive transient.

3 Theoretical Discussion

We analyze the data in terms of a time domain model of transient radiation from antennas. The model is based on concepts found in the antenna literature [6,7,8]. Our objective is to relate the main domain related features in the data to the structure of the antenna and the shape of the drive pulse. Only the main elements of the model will be presented here. The details will be published elsewhere.

We begin by assuming there are two distinct radiation mechanisms [6]-a traveling wave mechanism for the initial transient and a standing wave mechanism for the longer time oscillatory radiation. We analyze that the radiation received in the far field results from the transient and oscillatory photo induced currents in the antenna. A geometric construct is used to simplify the analysis as show in Figure 3 (a). First we consider the traveling wave radiation in the ideal dispersionless case for a step excitation. The excitation propagating from the source radiates continuously as a result of the accelerating charge at the step [8]. The sign of the radiation reverses at time $t = \frac{L}{C}$ due to reflection from the end of the

antenna. For an observer in the far field along the endfire direction, $\theta = 90^o$, the retarded field will have the form shown in Figure 3 (b). The response function for a square pulse is obtained by superimposing the step response with its inverse delayed by the pulse duration as shown in Figure 3 (c). If $L/c(1 - cos\varphi) << \tau_p$ pulse width, we may approximate the response function with delta functions as shown in Figure 3 (d). Convolving the response function with small reflection with a gaussian pulse yields 3 (e) which conforms with the analytical and numerical (moment method) results obtained for a "reflectionless" linear antenna.

The standing wave contribution results from the acceleration of charge due to reflection at the edge of the antenna. The broadside response function for an ideal dispersionless lossless delta function excitation is shown in Figure 4 (a). Reflection losses may be modeled with a reflection coefficient as shown is Figure 4 (b). Thus the total despersionless response function has the form:

$$f(t) = A \sum_{o}^{n=2} (-1)^n \, \delta \, (t - nT_1) - \text{traveling wave} \quad \text{eqn 1}$$

$$f(t) = A \sum_{o}^{n} (-1)^n (1 - r)^2 \, r^{2n} \, \delta \, (t - nT_2) - \text{standing wave} \quad \text{eqn 2}$$

Where:

$$T_1 = \tau_p = \text{width of photoconductive pulse}$$

$$T_2 = \frac{2L}{Ceff}$$

$$2L = \text{length of antenna}$$

Ceff = effective velocity of light in material

The measured far field traveling wave response is predicted by twice convolving the response function of equation 1 with a gaussian fucntions representing the photoconductive

pulse shape. Similarly, the measured far field standing wave response is predicted by twice convolving equation 2 with the same photoconductive pulse. The total measured response is the sum of the traveling wave response and the standing wave response delayed by the difference in propagation times in the antenna. The calculated response based on the above model is shown in Figure 5 (a), 5 (b), and Figure 5 (c). The model yields excellent overall agreement with the data.

Reexaming the data in the light of the model, one obvious difference between the LTSA and ETSA responses becomes apparent; the double hump in the initial portion of the LTSA response. Our model indicates that the underlying origin of this feature is that the delay between the traveling wave response and standing wave response in LTSA is greater than the corresponding delay in the ETSA. This suggests that the traveling wave in the LTSA experiences greater wave guiding despersions and, hence, travels at a slower velocity.

4 Conclusions

We have demonstrated the concept of planar optoelectronic picosecond tranceivers comprised of photoconductively driven tapered slot antennas. The far field transmitter response is composed of two distinct components: a traveling wave component and a standing wave component. The response can be accurately modeled in the time domain using simple geometric constructs. The resulting response functions may be used to predict the response to an arbitrary excitation waveform. Such antennas provide a unique opportunity for studying a variety of electromagnetic transient scattering problems as well as an entirely new method for characterizing antennas and guiding structures in the ultrafast time domain.

The authors gratefully acknowledge stimulating discussions with D. Schaubert, D.

Pozar, S. Yngvesson. This work was directly supported by the Air Force Office of Scientific Research. (Grant # AFOSR-84-0377) Additional support for our general efforts were provided by the National Science Foundation (Grant # NSFECS-8404495) and the Massachusetts Regents Fellowship Program.

5 References

1. D. H. Auston, K. P. Cheung, and P. R. Smith, Appl. Phys. Lett., 45, 284, (1984).

2. J. R. Karin, P. M. Downey, and R. J. Martin, IEEE J. of Quantm. Electrns., QE-22, 677, (1986).

3. A. P. DeFonzo, C. Lutz, and M. Jarwala, IEEE/OSA Conference on Picosecond Electronics, Tahoe, (1987).

4. K. L. Sala, G. A. Kenney-Wallace, and G. E. Hall, IEEE J. of Quantm. Electrncs., QE-16, 990, (1980).

5. D. H. Auston, A. M. Johnson, and J. C. Bean, Appl. Phys. Lett., 37, 371, (1980).

6. D. L. Sengupta, and C. T. Tai, Transient Electromagnetic Fields, Ed. L. B. Felson, (Springer-Verlag, New York, 1976).

7. D. H. Schaubert, Measurements of the Impulse Response of Communication Antennas, Harry Diamond Laboratory-Technical Report-1832, Nov. (1974).

8. G. Franschetti and C. H. Papas, IEEE Trans. on Ant. and Prop., AP-22, 651 (1974).

6 Figure Captions

Figure 1. Schematic of experimental configuration using matched optoelectronic antenna pairs. Dotted line indicates Exponentially Tapered Slot Antenna (ETSA). Solid line indicates Linearly Tapered Slot Antenna (LTSA). The pump pulse excites the transmitter at time t and the probe pulse samples the receiver at $t + \tau$.

Figure 2. (a) Correlation trace of LTSA with the transmitter and receiver on separate substrates. (b) Correlation trace of the ETSA with transmitter and receiver on separate substrates. (c) Correlation trace of ETSA with transmitter and receiver on a common substrate showing the isolated traveling wave component. The dotted line in (a), (b), and (c) is the autocorrelation trace of the independently measured photoconductive transient response.

Figure 3. Traveling wave response function analysis.

Figure 4. Standing wave response function (a) for lossless case (b) with reflection coefficient r used to model losses.

Figure 5. Calculated response based on the theoretical model for (a) LTSA (b) ETSA (c) Traveling wave component.

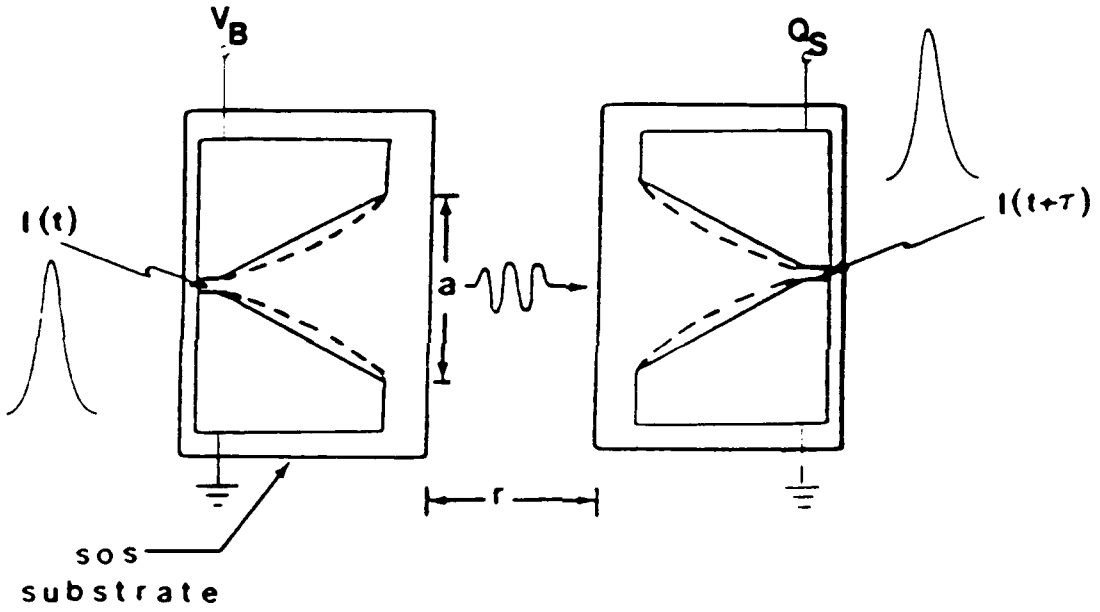
V_B
Q_S
I(t)
I(t+τ)
a
r
sos
substrate

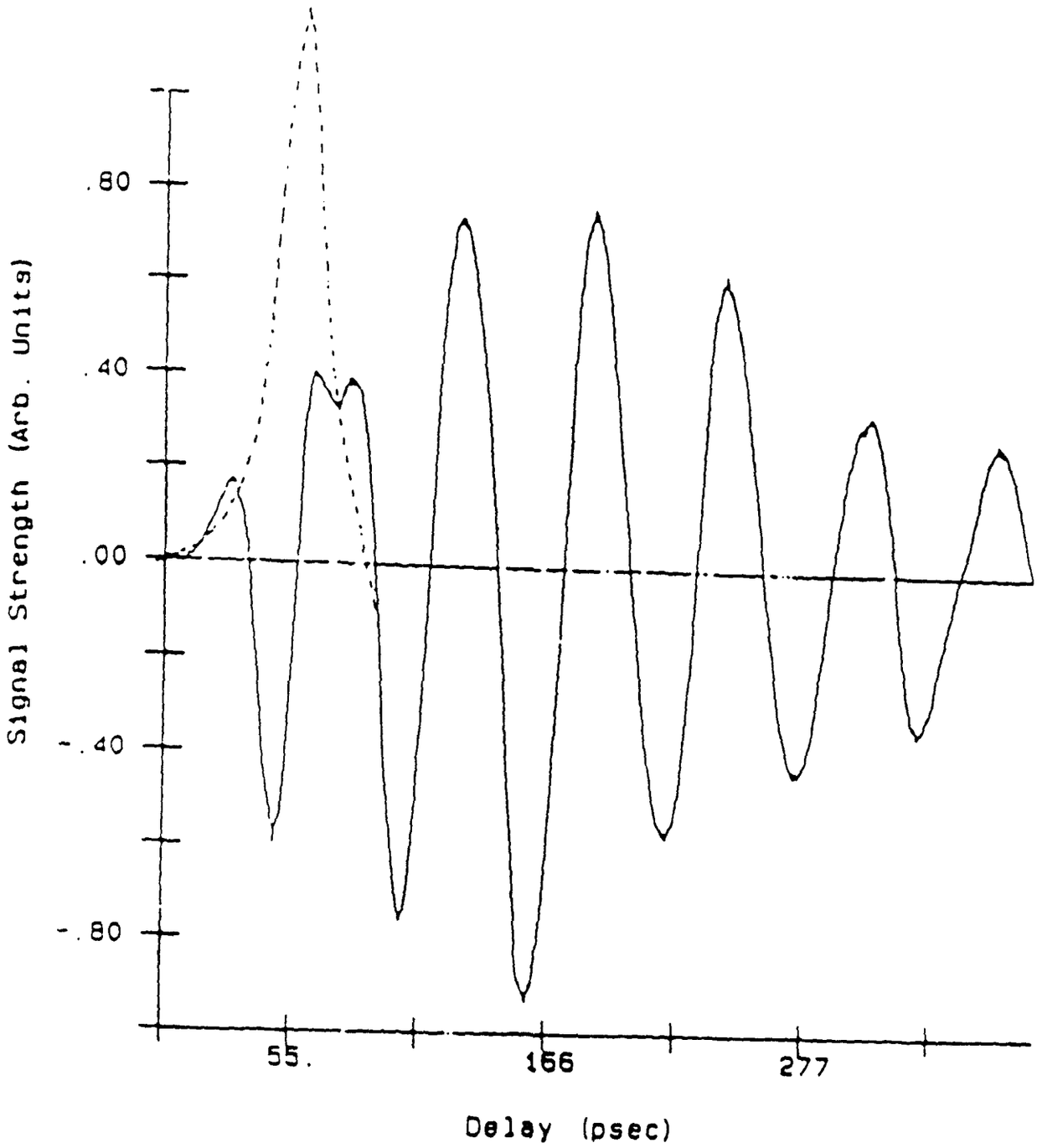

(a)

Signal Strength (Arb. Units)
-.80
-.40
.00
.40
.80
55
96
277
387
498
Delay (psec)
(b)

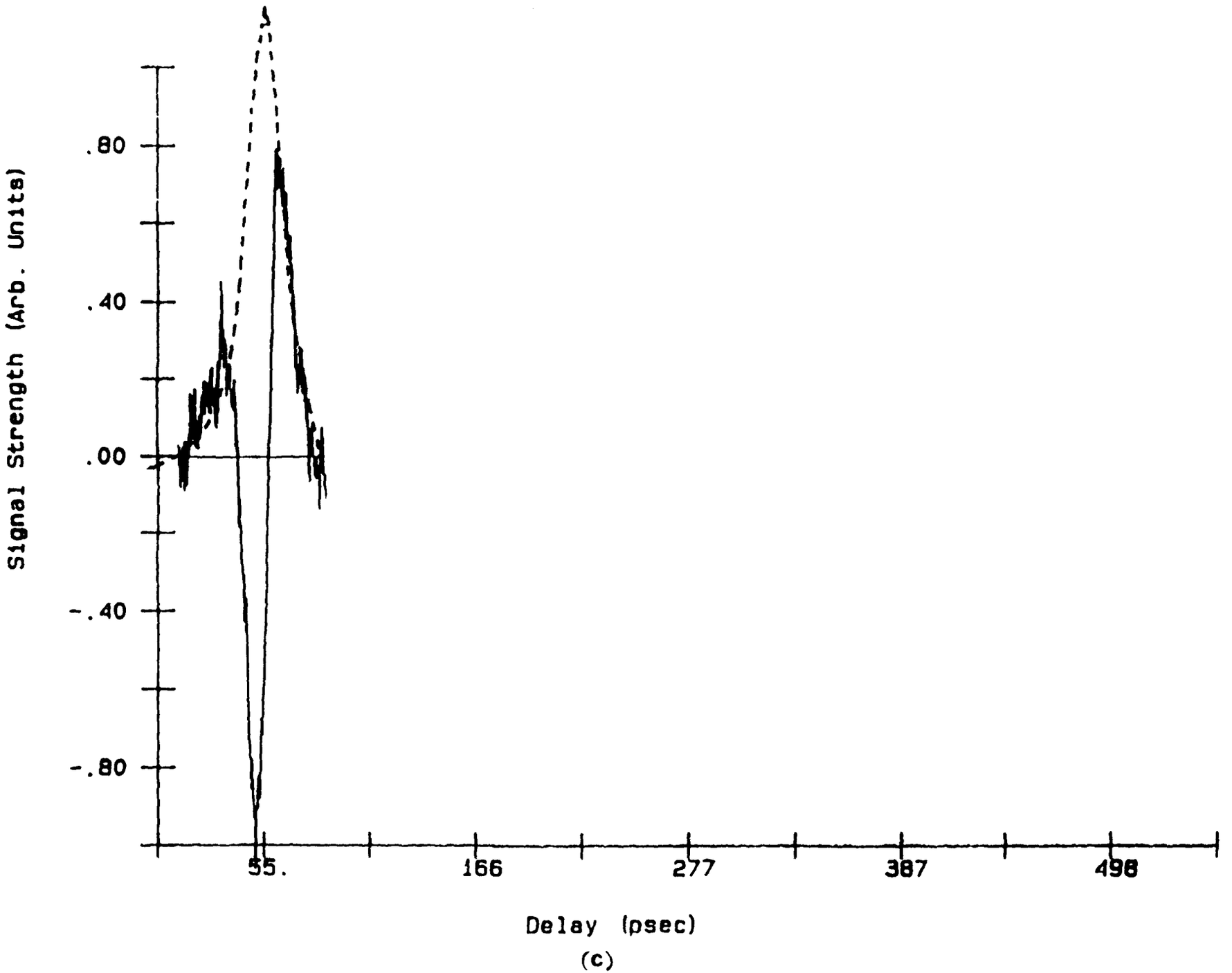
Signal Strength (Arb. Units)
.80
.40
.00
-.40
-.80
55.
166
277
387
498
Delay (psec)

(c)

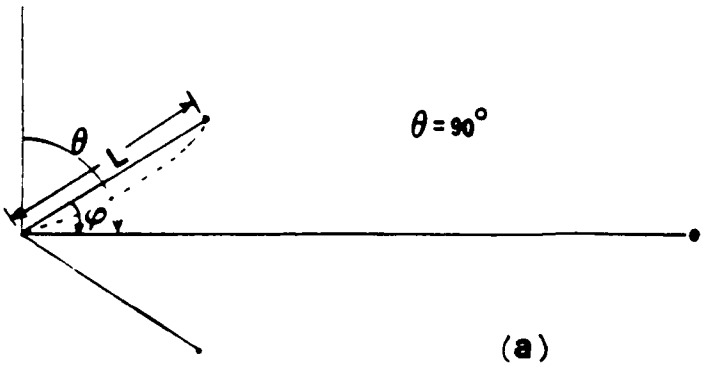

(a)

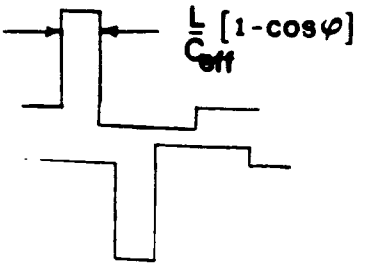

(b)

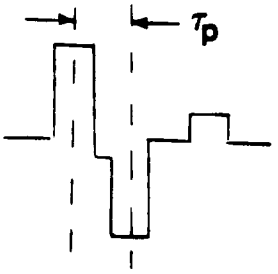

(c)

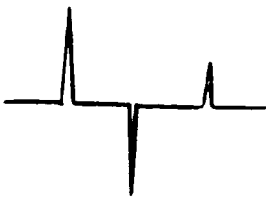

(d)

(e)

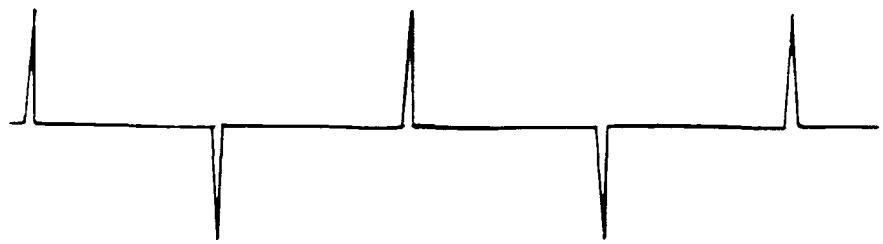

(a)

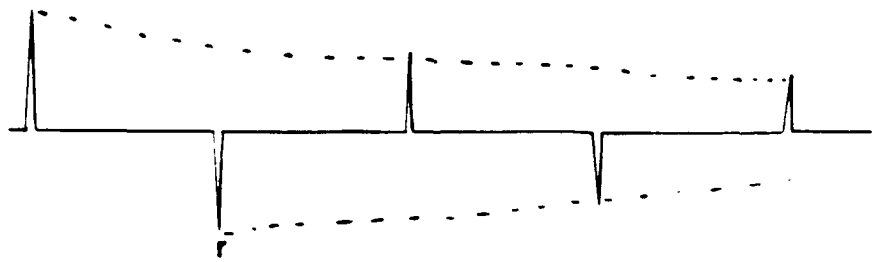

(b)

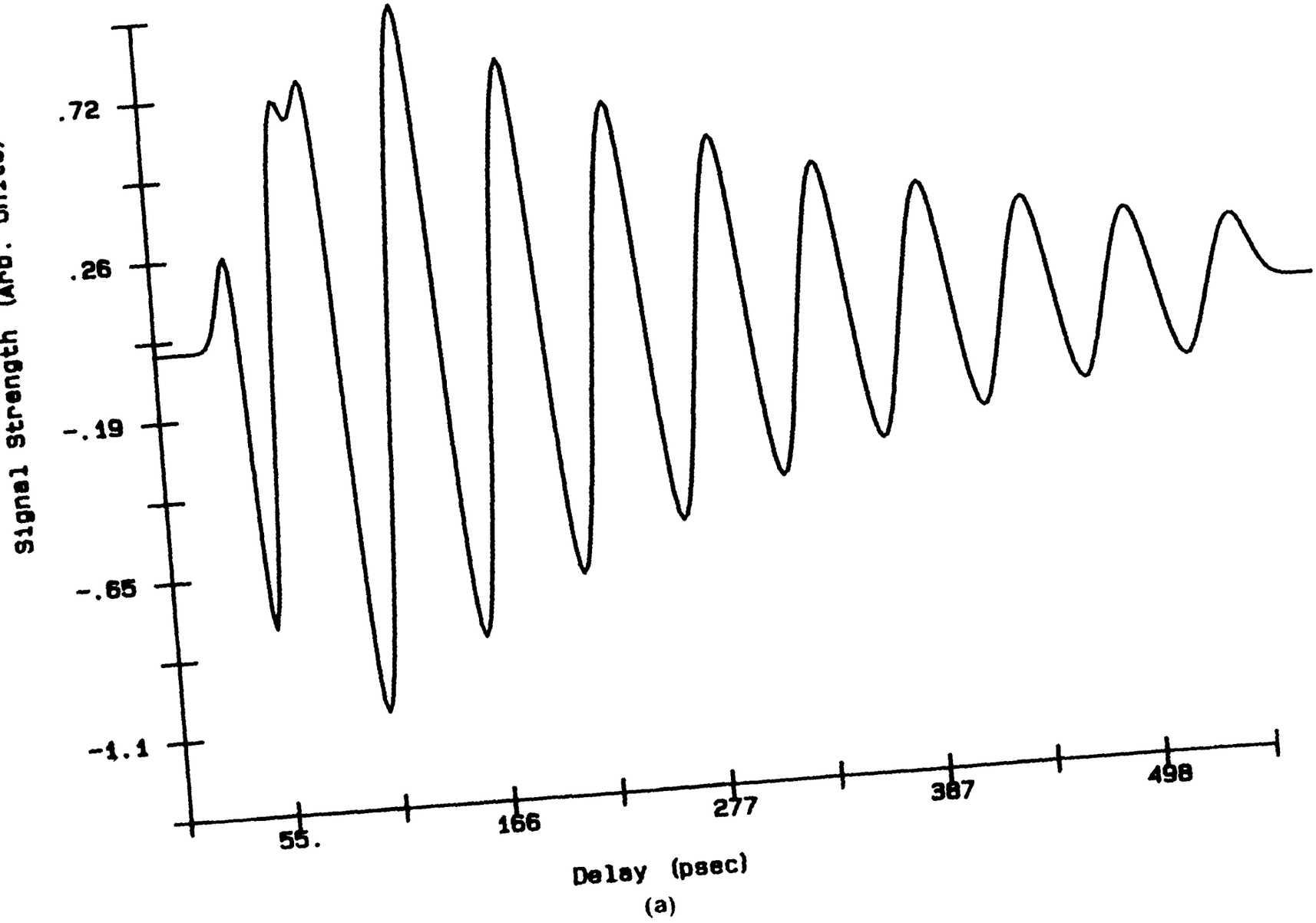
Signal Strength (Arb. Units)
.72
.26
-.19
-.65
-1.1
55.
166
277
387
498
Delay (psec)

(a)

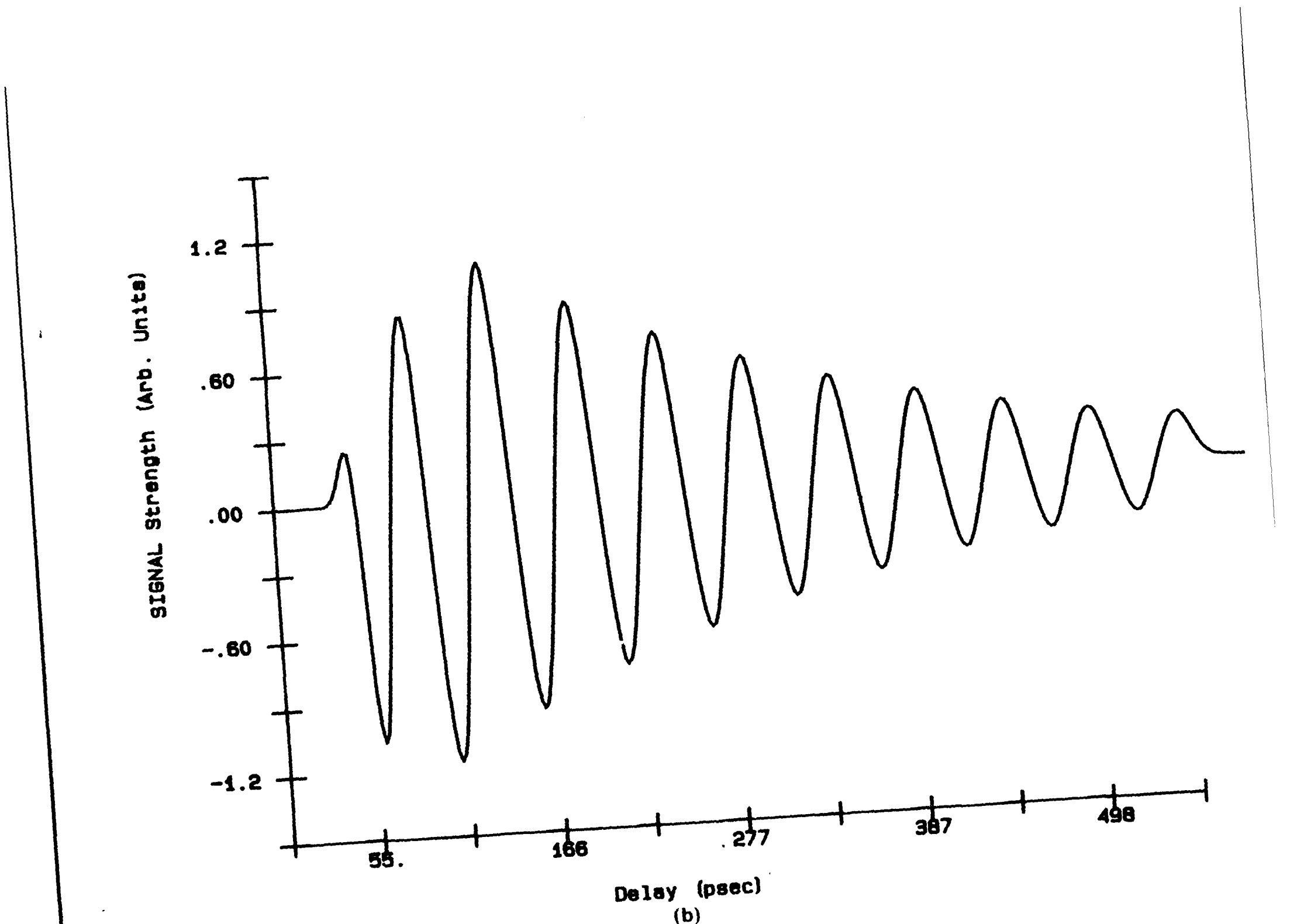
SIGNAL Strength (Arb. Units)
1.2
.60
.00
-.60
-1.2
55.
166
277
387
498
Delay (psec)

(b)

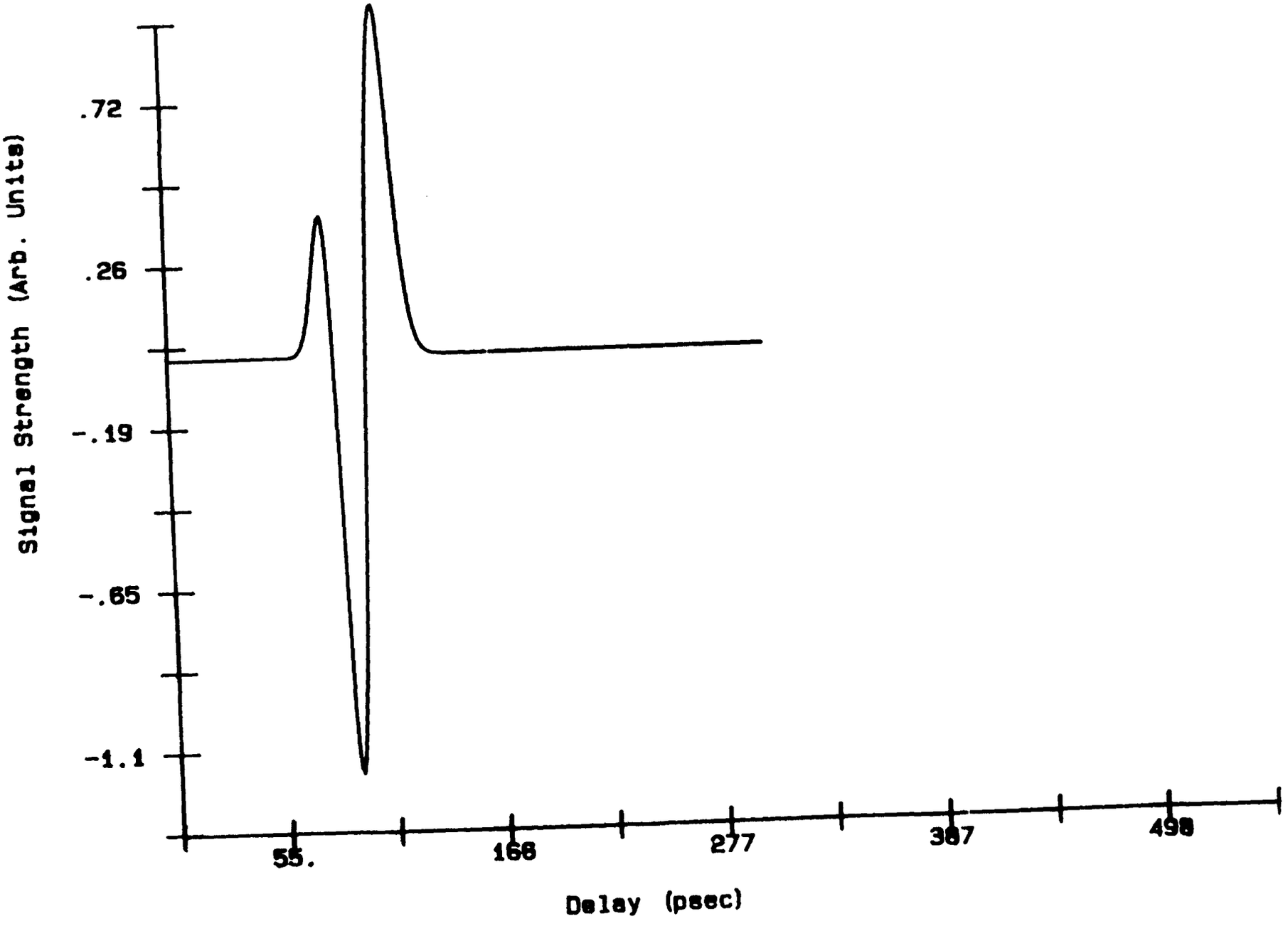
Signal Strength (Arb. Units)
.72
.26
-.19
-.65
-1.1
55.
168
277
387
498
Delay (psec)

(c)

Submitted CLEO/IQEC 87
Accepted
11/17/86

Radiation From Optoelectronic Antennas

Alfred P. De Fonzo, Madhuri Jarwala and Charles Lutz
Department of Electrical and Computer Engineering
University of Massachusetts, Amherst MA 01003
413-545-2374

Abstract:A model is presented that accurately predicts the time dependence of the electromagnetic impulse response of integrated optoelectronic linear antennas driven by picosecond photoconductivity.

Picosecond and subpicosecond photoconductivity is increasingly being used to generate short burst of electromagnetic radiation. In the most recently reported experiments , radiation was both transmitted and received photoconductively using well defined linear antennas [1,2]. Typical waveforms measured in the far and near fields are shown in Figure 1. Also shown is the independently measured autocorrelation trace for the photoconductive transient driving the transmitter. The antenna structure that generated the waveform in figure 1 is shown in figure 2. To predict the response of the antenna to picosecond photoconductive pulses we replace the tapered slot line antenna with a "bent" linear wire antenna as shown. The impulse response function is obtained by considering the radiation due to a square pulse which propagates from the generator to the wire ends and back again. There are two principle sources of radiation. The first source is the acceleration of charge at the front and back end of the propagating current pulse . From direct analysis in the time domain, the far field traveling wave response function for this source is found to be :

$$f(\tau)=A(n)\sum_{N=0}^{2}(-1)^{n}\exp\left[\frac{-(\tau-nT_{1})^{2}}{2\epsilon_{2}}\right]\times\left[1+\operatorname{erf}\left[\frac{\tau}{\sqrt{2\epsilon_{2}}}+\sqrt{\frac{2}{\epsilon_{2}}}nT_{1}\right]\right]$$

The second source is the acceleration of charge resulting from the reflection of the driving pulse from the antenna ends. The far field standing wave response for a square current pulse is then:

$$f(\tau) = C \sum_{n=0}^{N} (-1)^n (1-r^2)\, \gamma^{2n} \sqrt{\frac{\epsilon_2}{2}} \exp\left[\frac{-(\tau - nT_1)^2}{2\epsilon_2}\right]$$

$$\times \left[1+\operatorname{erf}\left[\frac{\tau}{\sqrt{2\epsilon_2}} + \sqrt{\frac{2}{\epsilon_2}}\, nT_2\right]\right]$$

Where τ =delay time, $T_1 = \tau_\rho$ = width of the photoconductive pulse assuming a gaussian shape, T_2 = the transit time of the pulse from the generator to the end of the antenna.
The transmitted response to a given pulse excitation is obtained by convolution with the gaussian photoconductive pulse. Twice convolving obtains the receiver response. The calculated results

for a linear tapered slot antenna excited by a gaussian pulse are shown in figure 3. Comparison with figure 1 demonstrates the excellent agreement between experiment and the model. Given the overall dimensions of an antenna and the shape of the driving pulse , the model can accurately predict the broadside waveform of both the transmitted and received signals. The model is being extended to non-broadside geometries. In conclusion , we have developed a model of the transient response of monolithic slot line antennas driven by picosecond photoconductive transients. Such models will be useful in the development of devices suitable for the optical generation , control and sensing of millimeter and submillimeter waves.

REFERENCES

1. A.P. DeFonzo, C.Lutz, and M. Jarwala,-accepted for presentation and publication, IEEE/OSA Conference on Picosecond Electronics, TAHOE, (1987)

2. A.P. DeFonzo, M. Jarwala, and C. Lutz, -Applied Physics Letters, submitted for publication

3. A.P. DeFonzo , M. Jarwala, and C.Lutz, IEEE Transactions on Antennas and Propagation-to be submitted

FIGURE CAPTIONS

Figure 1. (a) correlation trace of LTSA with transmitter and receiver on different substrates separated by a gap. Dotted line -photoconductive autocorrelation trace. (b) correlation trace of ETSA showing travelling wave component.

Figure 2. (a) Linearly tapered slot antenna showing contructions for determining impulse response function. (b) Travelling wave response function. (c) Standing wave response function.

Figure 3. Calculated response for LTSA with gaussian input pulse based on the theoretical model desribed in text.

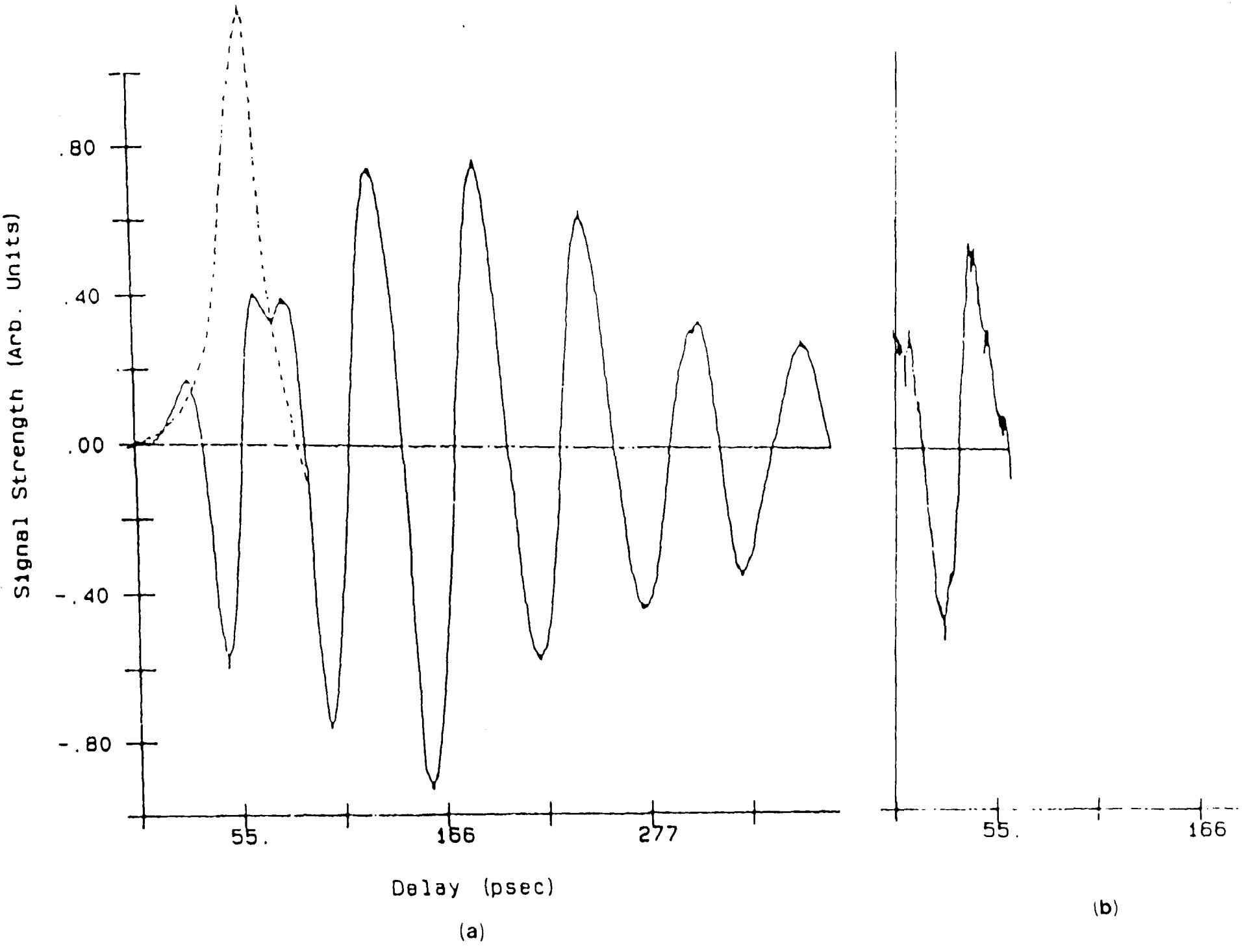
.80
.40
.00
-.40
-.80
Signal Strength (Arb. Units)
55.
166
277
Delay (psec)
(a)
55.
166
(b)

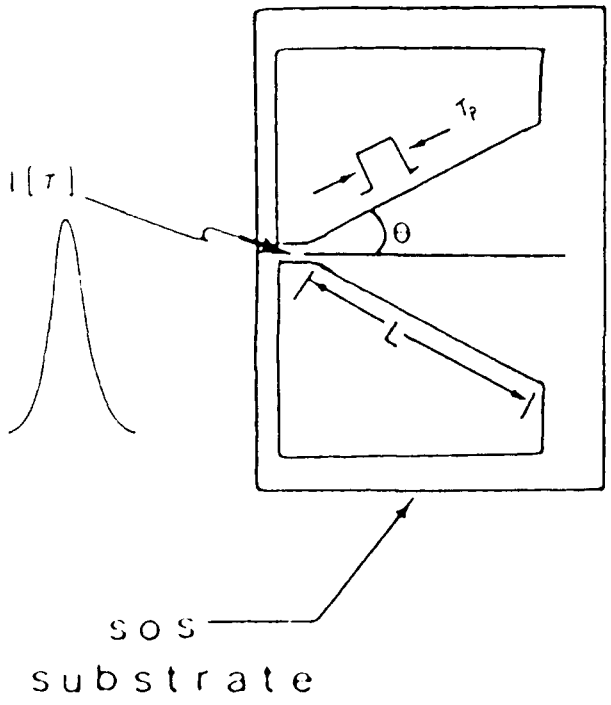

(a)

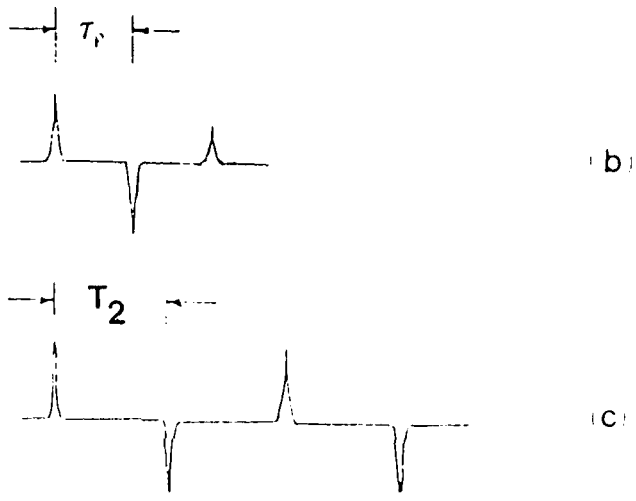

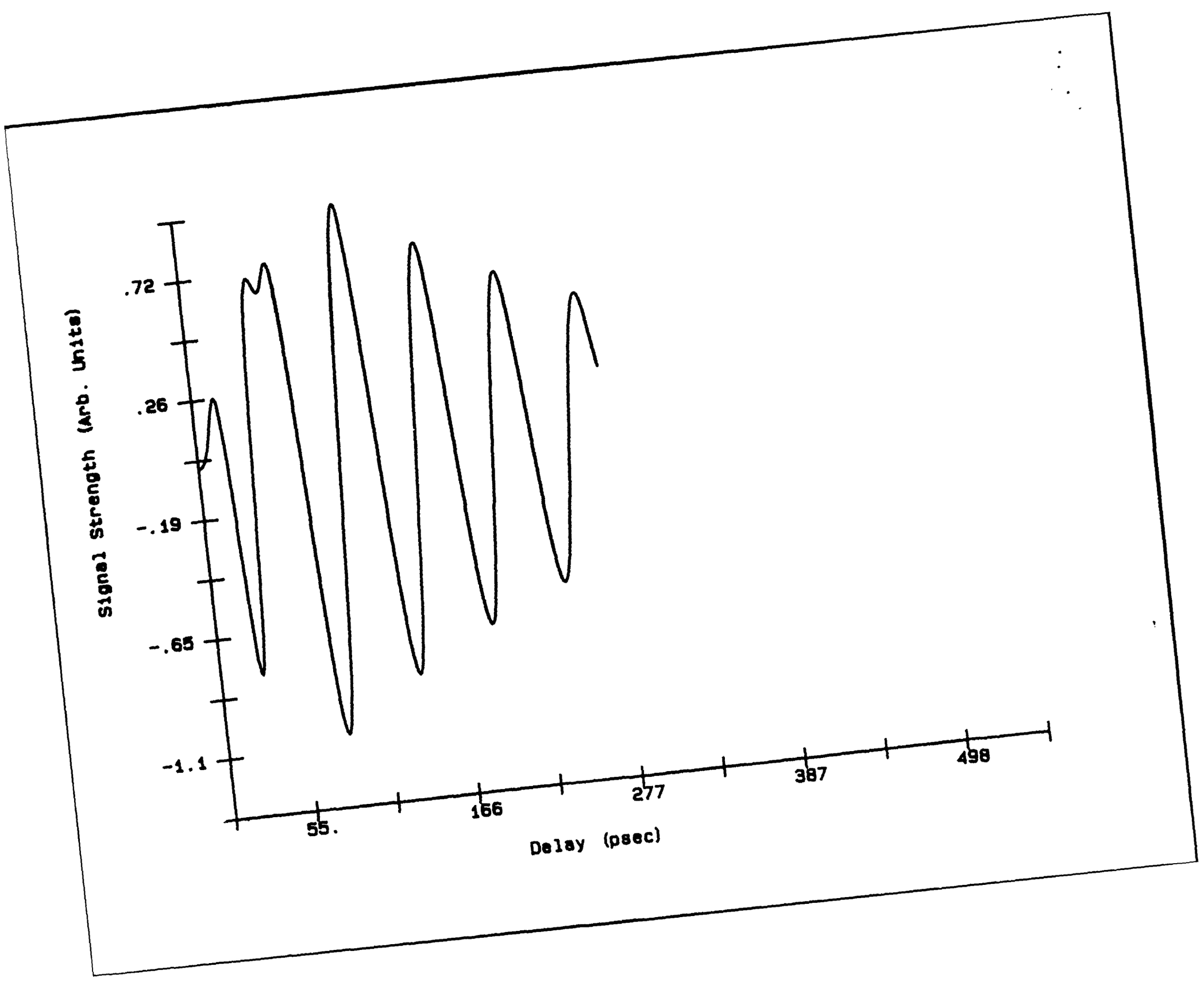
Signal Strength (Arb. Units)
.72
.26
-.19
-.65
-1.1
55.
166
277
387
498
Delay (psec)

Submitted CLEO/IQEC F7
Accepted.
6/17/96

Generation and Sensing of Millimeter Waves with Ultrafast Optoelectronic Integrated Antenna Elements

Alfred P. De Fonzo, Madhuri Jarwala and Charles Lutz
Department of Electrical and Computer Engineering
University of Massachusetts, Amherst MA 01003
413-545-2374

ABSTRACT: The development of broadband tapered slot antennas monolithically integrated on ion damaged silicon on sapphire substrates that were used to transmit and receive optically generated centimeter/ millimeter wavelength radiation is reported.

Using new integrated photoconductive slot antennas, we demonstrate for the first time the generation and sensing of both short burst and quasi continuous radiation spanning the millimeter wave bands. The devices efficiently generate radiation in the far field with bias voltages in the 1 -50 volt range and optical pulse energies in the pico and subpicojoule range. The photoconductively sampled receiver senses the transmitted radiation in the far field with excellent signal to noise ratio using a 100 Mhz sampling rate.

Previous schemes for generating and sensing picosecond burst of millimeter wave radiation in small scale semiconductor devices evolved from the study of unexpected spurious radiation from microstrips or discontinuity in microstrips in non planar geometries not necessarily optimized for radiation [1,2]. The devices presented here are based on planar integrated waveguide and antenna technology [3]. Such waveguides afford ease in optical coupling and have potential instantaneous electrical bandwidths from dc to greater than a terahetz.

Our initial work was on closely coupled transceivers on a common substrate [4]. Here we report the results of characterizing optoelectronic millimeter wave transceivers with the transmitter and the receiver on different substrates separated in space . The basic configuration of the devices is shown in Figure 1. Each tapered slot antenna is formed from an aluminum film deposited on a silicon on sapphire substrate. The substrate was prebombarded with O+ ions at 100 Kev and 200Kev to dosages of 10^15 / cm^2. Standard photolithographic techniques were used to etch the antenna pattern in the thermally evaporated aluminum film. The feed end of the slot antenna was 30 microns wide and the aperture end was 2.9 mm wide. Two forms of tapers were investigated : an exponentially tapered slot antenna (ETSA) as indicated by the dotted line in Figure 1 ; and, a linear tapered slot antenna (LTSA).

The transceiver is operated by exciting the biased feed slot of the transmitter with a short optical pulse at time t and sampling the receiver output slot with a short optical pulse at a delayed time $t+\tau$. The waveform is determined over all time by sampling over a range of τ .

The sampled waveform for a LTSA transmitter and receiver spaced 1cm apart is shown in Figure 2. The data was taken with 2 picosecond optical pulses from a modelocked dye laser. The transmitted signal is composed of an initial fast transient followed by a quasi continuous damped oscillation of much lower frequency. The quasi continuous radiation can be suppressed by matching the end points of the antenna into a slot line. The data can be accurately predicted using a model response fuction derived from antenna theory [5].

The present device demonstrates the potential for optical generation, control and sensing of millimeter waves using technology that may be easily incorporated into existing monolithic fabrication procedures.

REFERENCES

1. D.H. Austin, K.P. Cheung, and P.R. Smith, Appl. Phys. Lett., 45,p284-286, (1984)

2. J.R. Karin, P.M. Downey, and R.J. Martin, IEEE J. of Quantm.Electrns., Qe-22, p677-681,(1986)

3. Nan-Lei Wang, and S.E. Schwarz,Int. J. of Infrared and Millimeter Waves, Vol 3,#6,p771-782,(1982)

4. A.P. DeFonzo, C.Lutz, and M. Jarwala-IEEE/OSA Conference on Picosecond Electronics,TAHOE (1987)

5. A.P. DeFonzo, M.Jarwala, and C. Lutz; Applied Physics Letters, submitted for publication

FIGURE CAPTIONS

Figure 1. Optoelectronic transmitter and receiver on individual substrates separated in space. Solid line indicates LTSA. Dotted line indicates ETSA (see text)

Figure 2.(a) Correlation trace of LTSA with transmitter and reciever on separated substrates. Dotted line is the autocorrelation trace of theindependently measured photoconductive transient response. (b) Correlation trace of ETSA showing the isolated travelling wave component.

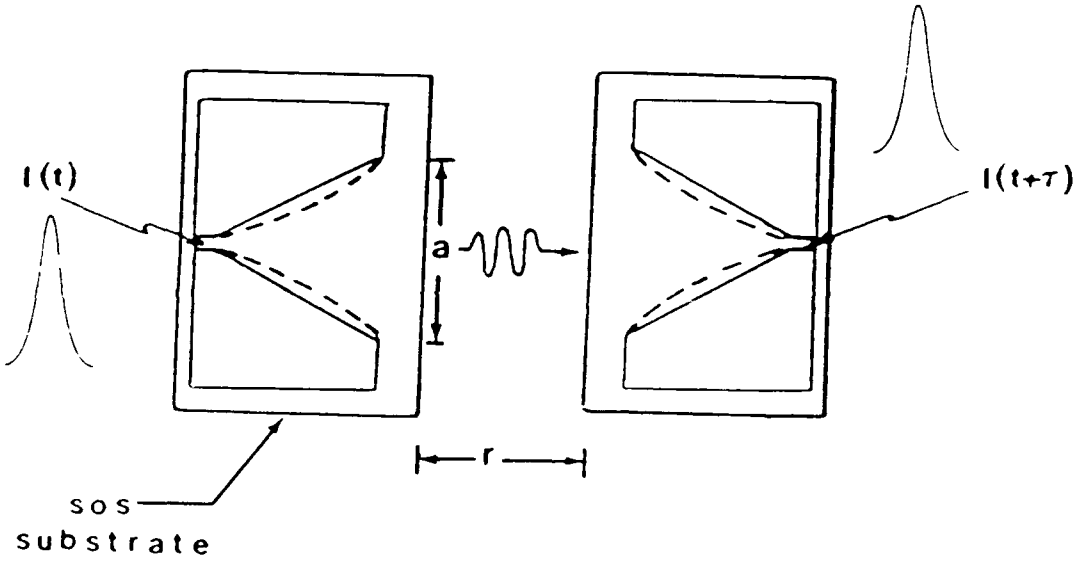
I(t)
a
I(t+τ)
r
SOS
substrate

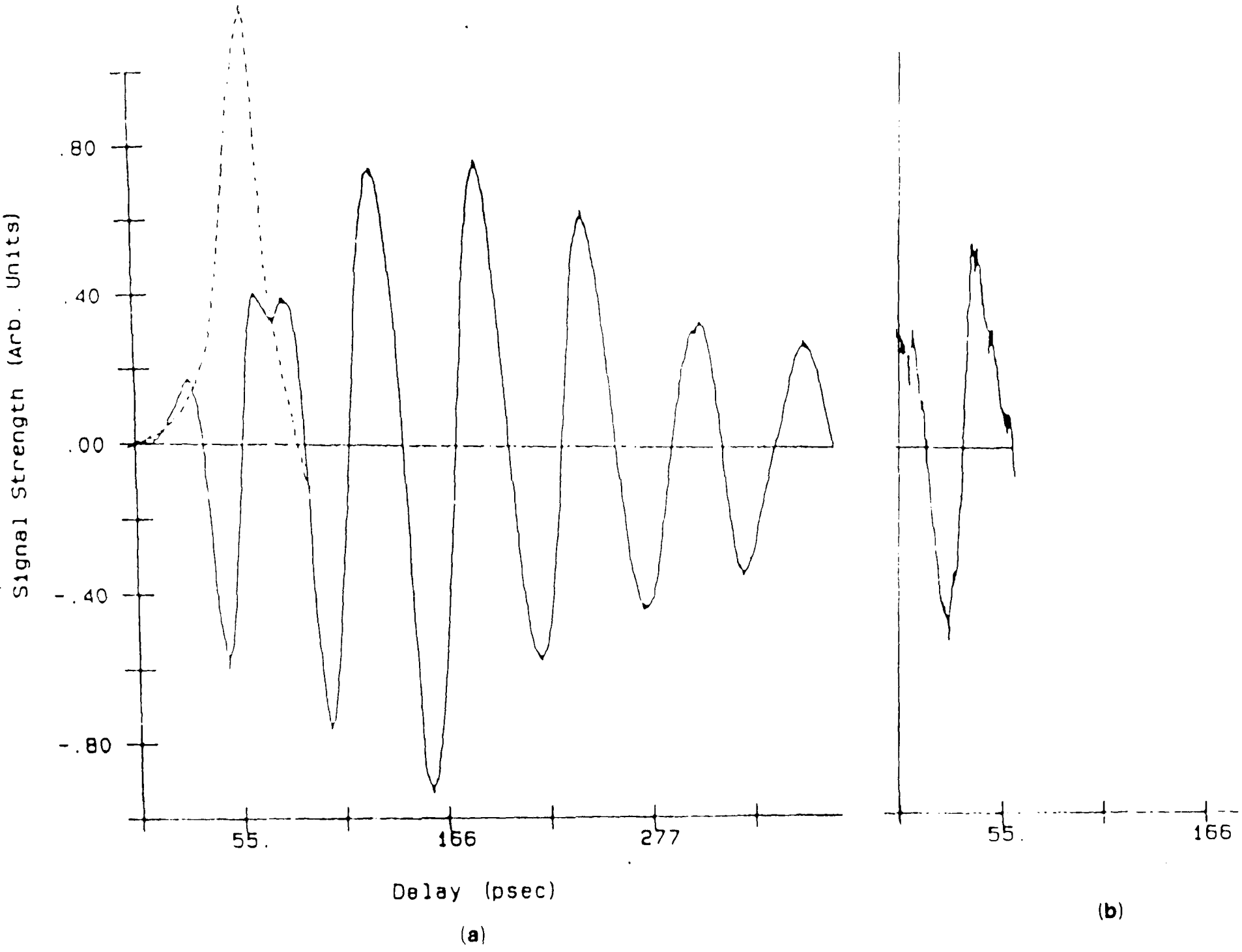
.80
.40
.00
-.40
-.80
Signal Strength (Arb. Units)
55.
166
277
Delay (psec)
(a)
55.
166
(b)

Optoelectronic Transmission and Reception of Ultrashort Electrical Pulses

Alfred P. DeFonzo and Charles R. Lutz

Department of Electrical and Computer Engineering
University of Massachusetts, Amherst, Ma 01003
(413) 545-2374

1. Abstract

We report on the recent advances in using integrated planar antenna technology to photoconductively generate and detect picosecond radiation. Detection of a single pulse of picosecond duration has been achieved using a coplanar antenna structure fabricated on a radiation damaged silicon-on-sapphire substrate.

2. Introduction

Recent experiments have shown that fast optoelectronic switches monolitically integrated with an appropriate guiding structure can be used to generate, control, and, detect picosecond bursts of electromagnetic radiation [1,2,3]. Potential advantages of such devices include the ability to transmit wide bandwidth electrical signals with limited distortion caused by dispersion and other frequency-dependent losses, the capability of integration with existing millimeter wave circuits, and the ability to provide optical interfaces to these circuits. Such devices should prove useful as samplers and electrical interconnects in various millimeter wave applications. However, in order to control the spatial and temporal distribution of the radiated wavefront, it is necessary to employ more sophisticated antenna elements than simple gap discontinuities in microstrip transmission lines.

In our initial work[2,3], we demonstrated the concept of using a planar antenna structure deposited on radiation damaged silicon-on-sapphire substrates to transmit and receive transient radiation produced by photoconductive switches which were driven by picosecond laser pulses. A model which predicts the transient behavior of these antennas was also developed. Figure 1 shows the received signal obtained from this antenna structure and the inset is a schematic diagram of the device. This waveform consists of two components, an initial fast transient followed by an interval of long period, decaying oscillation. In this letter, we report on the results of experiments conducted using an entirely new class of optoelectronic antennas. The design was motivated by the need to develop a structure in which the radiated electric field was a replica of the optical pulse, free of any ringing or standing wave components[3]. The design was based on conclusions obtained from the modeling of the various radiation mechanisms in the recently reported structure and represents a significant advance in picosecond electronic technology. In addition,it is required that the device posses a flat, wide bandwidth frequency characteristic which would minimize any distortion of the propagating pulse. We show, for the first time that this can be accomplished with the use of low dispersion coplanar slot antennas.

3. Experiment

The geometry of the experiment is illustrated in Fig. 2. An exponentially flared coplanar transmission line, with a design impedance of 100 ohms, is formed from aluminum, deposited on ion bombarded silicon-on-sapphire substrates, using conventional photolithographic techniques. The overall length of the structure was 7.9 mm and the width of the aperture was 1.9 mm. The photoconductive generator consists of a relatively long, approximately 4 mm, section of transmission line. The lines are 12 um wide and separated by 25 um. This structure drives the

radiating element which is formed by flaring the remaining 4 mm of transmission line. The exponential flare was of the form W = 2Aexp(px), where W is the separation distance, x is the length parameter, and A and p are constants with values of 2.55 and 0.0263 respectively. The ratio of the separation distance, W along the flare to the width of the transmission line, w, was kept constant at a value of two. Sampling gaps placed along the length of the transmission line provide a means of determining, insitu, the shape of the actual photoconductive pulse driving the antenna.

The transmitting antenna is dc biased and can be discharged by photoconductively shorting the transmission line with a picosecond optical pulse via the "sliding contact" method [4]. The current pulse is guided into the antenna region where it radiates an electromagnetic field which is directed toward the opposing antenna. When the field reaches the receiving antenna, it impresses a transient bias voltage proportional to the strength of the field, across the gap of the transmission line. This voltage is photoconductively sampled by illuminating the semiconductor material between the gap with a second picosecond laser pulse derived from the same source as the pump pulse but delayed by a variable time tau. The functional dependence of the received signal is determined by varying the time delay over the duration of the transient. The width of the photoconductive pulses is controlled by bombarding the silicon epilayer with high energy O+ ions. Ion energies of 100 Kev and 200 Kev at dosages of 10 15 ions cm-2 were used in our experiments.

The optical pulses were produced from a synchronously pumped modelocked R6G dye laser pumped by a frequency doubled Nd:YAG laser operating at 1.06 um. The dye laser pulses had measured durations of approximately 2 ps at a wavelength of 580 nm and a 100 Mhz repetition rate. The average power was 12 mW for the pump beam and 47 mW for the probe beam. A standard pump and probe arrangement was used to obtain the experimental measurements[1-4]. The time delay between the pump and probe beams was controlled by mechanically positioning a retroreflector with a stepping motor. The pump beam was chopped at 1.5 Khz and a lock-in amplifier was used to detect the sampled photocurrent from the receiving antenna. The output of the lock-in was digitized and no signal averaging was necessary.

4. Results

Correlation measurements obtained for the field radiated by the new structures are shown in Fig. 3(a). The two antennas were separated by an air gap of approximately 0.7 cm and the spatial separation of the pump and probe beams was 2.3 cm. Transmitting and receiving antennas were identical, except the transmitter did not have the sampling structure.

Illustrated in Fig. 3(b) is the correlation trace of the photoconductive drive pulse. This signal was obtained by placing

the probe beam on the gap of the first sampler and the pump beam between this point and the bonding pads. The data clearly shows that the antenna structures do not introduce any significant broadening of the radiated pulse, indicating that the coplanar structure is a wide bandwidth configuration. The lack of any reflection components in the received signal imply that this structure has a high radiation efficiency and totally suppresses any standing wave component[3]. The insets in Fig.3 show the autocorrelation signal for the optical pulses. Figure 4 depicts the same data, except in this case the pump beam was focused between the two sampling arms as indicated in the inset. These results imply that the sampling arrangement used in these devices present a small impedance mismatch to the current pulse propagating down the transmission line.

Recently reported work [5] using a similar material has demonstrated the generation of photoconductive electrical pulses on the order of 600 fsec. These results support our previous conclusions and imply that our antennas can be directly used in the femtosecond regime.

5. Conclusion

In summary, we have shown that these new structures eliminate standing wave components in the radiated field and are extremely broadband. Furthermore, the radiated pulse was shown to be a replica of the optical excitation pulse and free of any distortion other than that caused by the inherent dispersion of the transmission line structure. This device exhibits electrical bandwidths in excess of 200 GHz and is one of the largest bandwidth antennas ever reported. We anticipate that with improved processing methods we will be able to generate and radiate sub-picosecond transients with these devices.

The authors wish to acknowledge the generous support provided by the Air Force Office of Scientific Research under grant number AFOSR-84-0377.

6. References

1. D.H. Auston, K.P. Cheung, and P.R. Smith, Appl. Lett.,45,284,(1984).

2. A.P. DeFonzo, C.R. Lutz, and M. Jarwala,Picosecond Electronics and Optoelectronics Technical Digest, 87-1(Optical Society of America, Washington, D.C. 1987) pp.40-41

3. A.P. DeFonzo, M. Jarwala, and C.R. Lutz, Transient Response of Planar Integrated Optoelectronic Antennas, submitted for publication to Appl. Phys. Lett.

4. M.B. Ketchen, D. Grischkowsky, T.C. Chen, C-C. Chi, I.N. Duling, N.J.Halas, Appl. Phys. Lett. 48,751,(1986)

5. D. Grischkowsky, C-C. Chi,I.N. Duling, W.J. Gallagher, N.J.Halas, J.M. Halbout,M.B. Ketchen, Picosecond Electronics and Optoelectronics Technical Digest, 87-1(Optical Society of America, Washington, D.C. 1987) pp.44-45

7. Figure Captions

Fig.1 Transient response of the original antenna configuration. The inset is a diagram of this structure.

Fig.2 Schematic of transmitter configuration. The receiver is identical except that no bias is applied.

Fig.3 (a) Correlation signal of the field radiated by the devices shown in Fig.1. The inset shows the autocorrelation of the exciting optical pulse.
(b) Correlation signal of the photoconductive drive pulse propagating on the coplanar transmission line. The inset shows the autocorrelation of the exciting optical pulse.

Fig.4 Correlation trace of the photoconductive drive pulse when the pump is placed between the sampling arms, as shown in the inset.

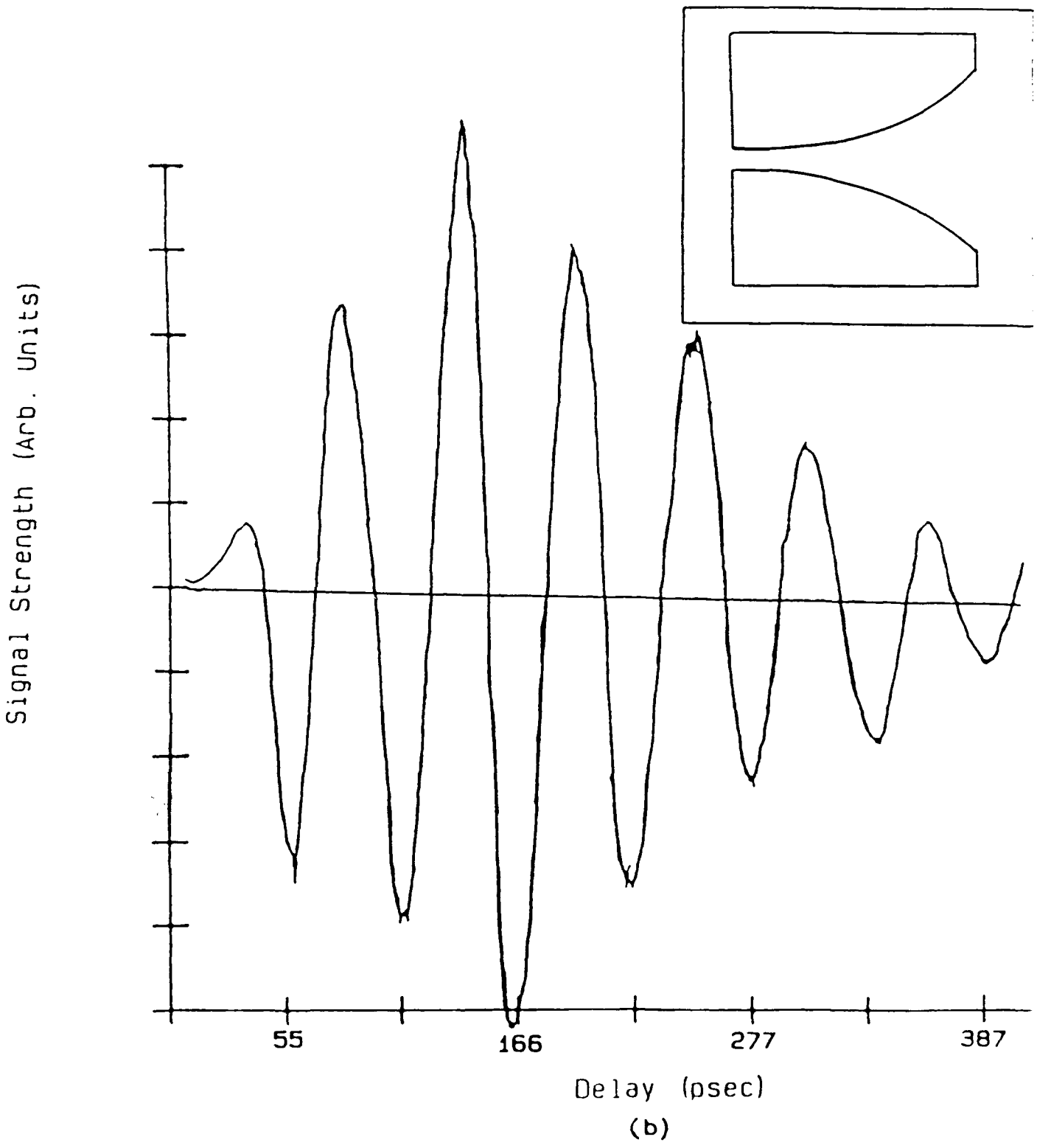

(b)

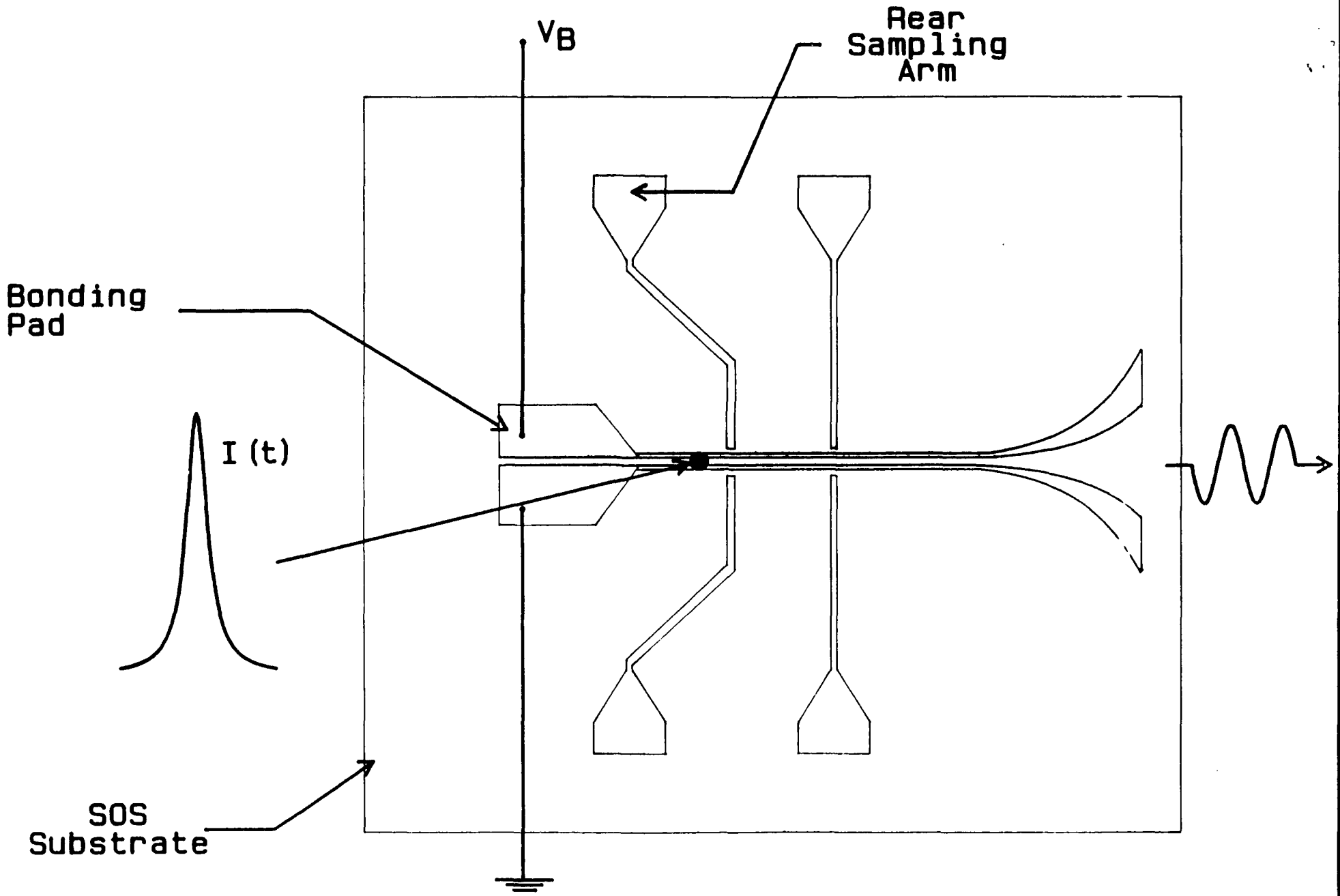
V_B
Rear
Sampling
Arm
Bonding
Pad
I (t)
SOS
Substrate

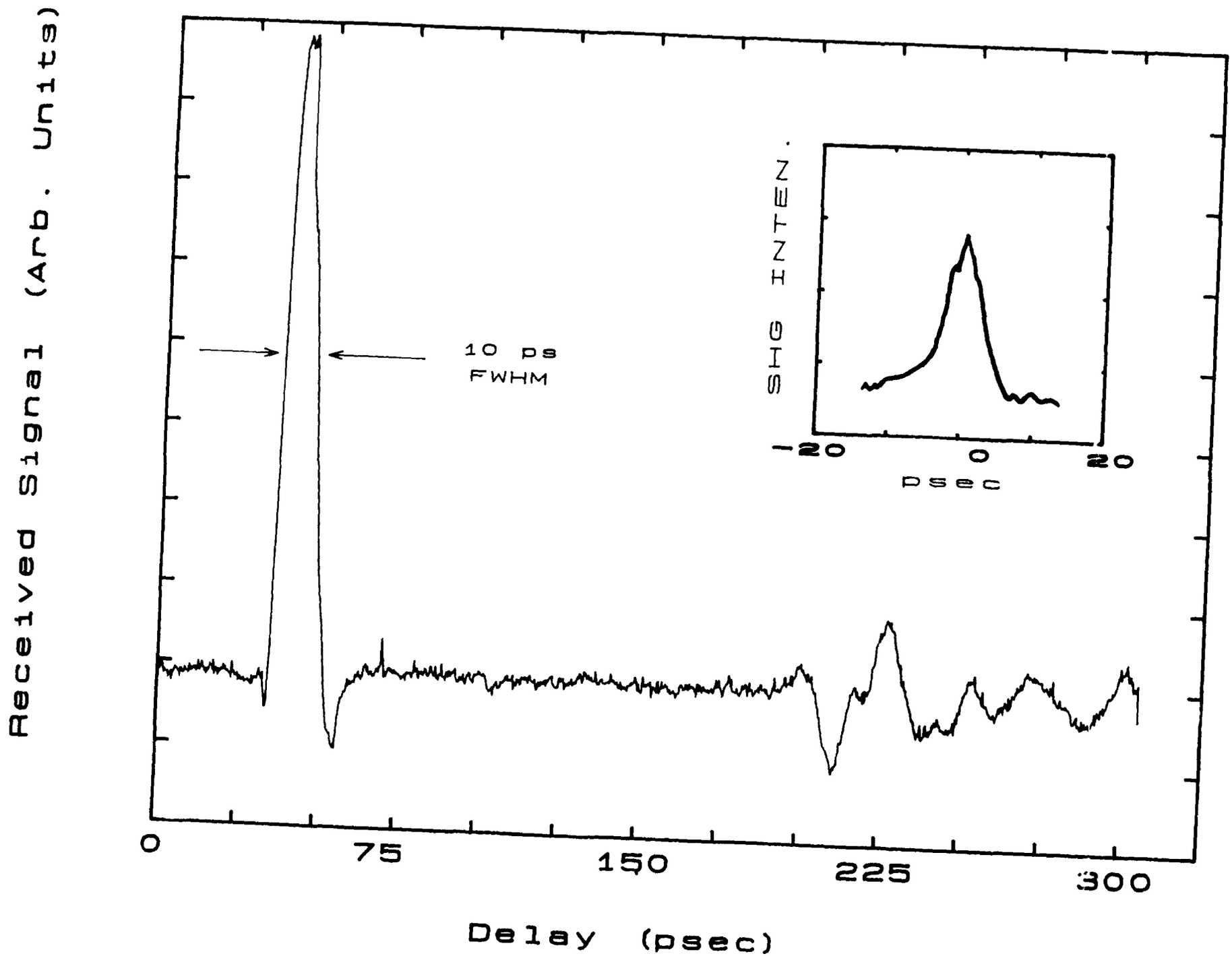
Received Signal (Arb. Units)
10 ps
FWHM
SIG INTEN.
-20
0
20
psec
0
75
150
225
300
Delay (psec)

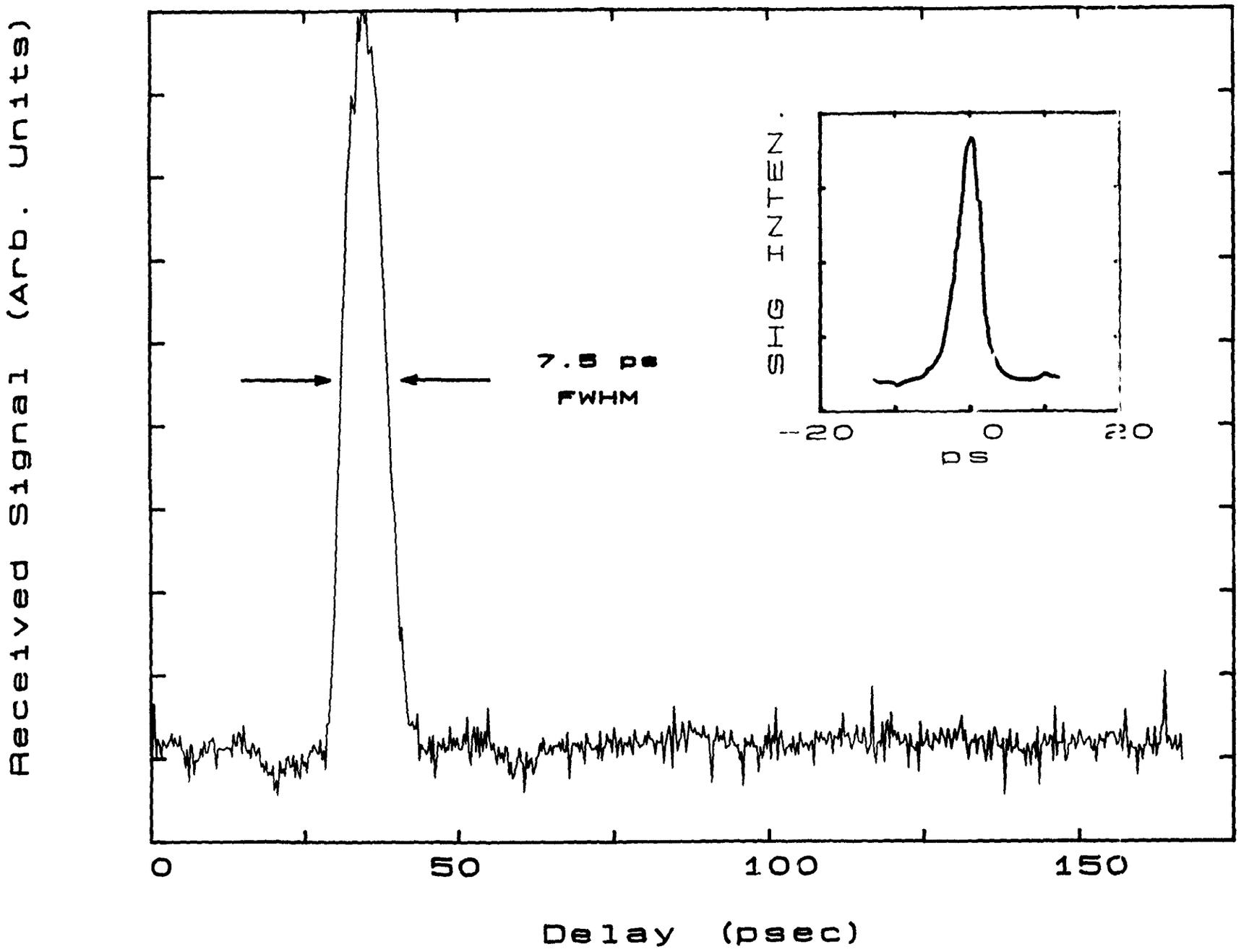
Received Signal (Arb. Units)
7.5 ps
FWHM
SHG INTEN.
-20
0
20
DS
0
50
100
150
Delay (psec)

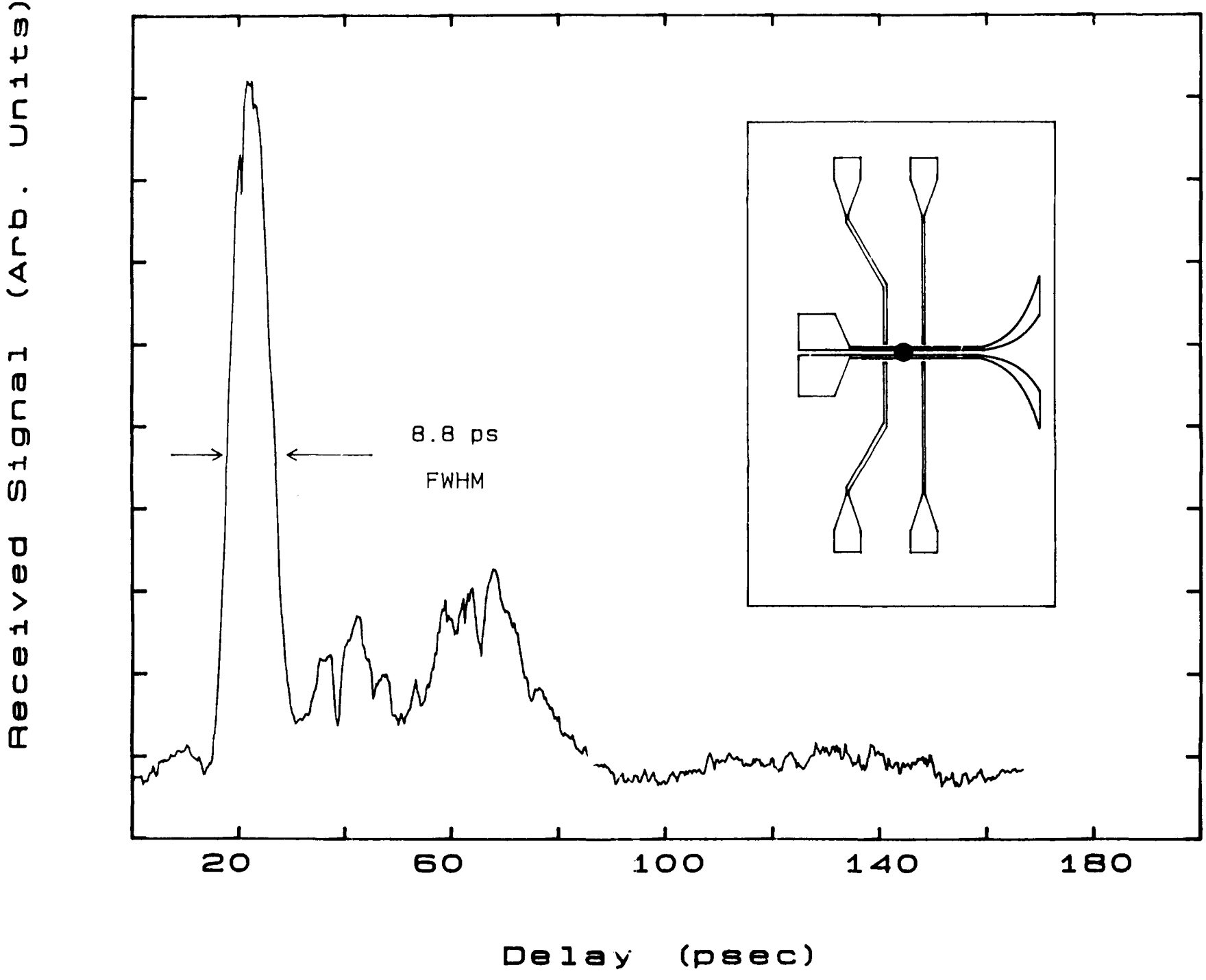
Received Signal (Arb. Units)
8.8 ps
FWHM
20
60
100
140
180
Delay (psec)

Submitted for publication
Optics Letters

Title and Abstract

Bistability, Self Phase Modulation and Stimulated Raman Scattering in Single Mode Fibers

Alfred P. DeFonzo and Neil Gitkind

Department of Electrical and Computer Engineering
University of Massachusetts, Amherst 01003

ABSTRACT

Standard telecommunication single mode fibers are found to exhibit bistable behavior when pumped by 90 psec 1.06 micron pulses with powers exceeding 150 W peak. The bistability is accompanied by a rapid change in the amount of self-phase modulation and stimulated raman scattering of the pump pulse. We estimate the nonlinear index response time $\tau_r = 1\text{x}10^{-15}$ and the relaxation time $\tau = 75_{PS}$ by attributing the bistability to transient self–focusing.

Introduction

It has been recently reported that the onset of transient Stimulated Raman Scattering (SRS)in single mode polarization preserving fibers is accompanied by the saturation of the output power of pump pulses launched into an optical fiber [1]. This saturation of output pump power is of immediate practical interest in achieving maximally chirped pulse power for subsequent pulse shaping and compression. Commercial pulse compressors achieve high output powers with circularly polarized light. In this letter we report the results of an investigation of self phase modulation and stimulated raman scattering using circularly polarized light and, in particular, we report the first observation , to our knowledge, of bistability in the output power of the pump pulses. The bistability is directly manifested in the intensity of SRS and the magnitude of pump chirp at some critical power. This effect is of practical interest as a limiting mechanism for pulse compression and as a mechanism for controlling or rapidly switching relatively large amounts of laser power.

It has been found that an intensity dependent refractive index imposes a linear frequency chirp on optical pulses propagating in fibers. These chirped pulses can be compressed by means of a dispersive delay line implemented with a diffraction grating pair [2]. When driving the fiber at high power levels, SRS is found to limit this process by first depleting the power in the chirped pulse and then altering the distribution of spectral components [3]. Many of the experiments to date have used single mode polarization preserving fiber. We have found that by driving standard telecommunications fiber with circularly polarized pulses whose center wavelength is 1.06 microns we could readily observe a discontinuous reduction in the chirped pulse power output at the onset of SRS. Here we present a detailed description of this surprising effect along with an analysis of the possible origins. The analysis of such effects can lead to a better understanding of the

nonlinear properties of fibers and interesting new applications.

Description of Experiments

Linearly polarized optical pulses from a Nd:YAG laser operated at a wavelength of 1.06 microns are converted into circularly polarized optical pulses and are coupled into a standard telecommunications fiber. The circularly polarized output is then converted back into linearly polarized light and passed through a Glan-Thompson prism polarizer with an escape window . Rejected polarization components can be monitored with a slow photodectector. The total transmitted pulse power is monitored by both a slow germanium diode and further resolved in the time domain with a high speed InGaAs photodetector (risetime= 35psec). The output pulses are then spectrally resolved with a grating spectrometer (ISA HR-320) and recorded with a photodiode array. The output pulses are further spectrally resolved with a holographic grating pair in Littrow configuration and the power at 1.06 microns monitored with a slow silicon photo diode. The spectrally and temporally resolved pulses are displayed on a Tektronix 7904 oscilloscope outfitted with a S-4 sampling head. Integrated intensities of the 1.06 micron pulse , and the total output power were plotted on an XY recorder after averaging with a lock–in amplifier. The input pulse was simultaneously monitored by the InGaAs detector. The pump pulses were 90 psec in duration [FWHM] and the average power could be continuously adjusted from 0 to 8 watts without significant change in fiber coupling by means of a prism polarizer and a rotating waveplate. Using a standard microscope objective and a mild prefocussing lens we achieved 60% coupling into the fiber.

In general, we were able, at high input powers, to observe spectrally broadened output pulses centered at 1.06 microns, 1.08 microns, 1.04 microns and 1.12 microns. The stokes-antistokes pair at 1.08/1.04 microns could be selectively induced by adjusting coupling .

This surprising effect is suppressed at maximum coupling and was thereby removed from the experiments. The results of an experimental analysis of stokes/ antistokes generation is reported elsewhere [4]. At low input powers the output power was observed to be in the commonly observed [2] form of linearly chirped pulses spectrally centered on 1.06 microns. At high input powers two pulses were observed , one centered at 1.12 microns and another at 1.06 microns. The 1.12 micron pulse exited in advance of the 1.06 micron pulse due to their different group velocities in the fiber. This "walk-off" phenomenon has been reported elsewhere [1,4,5].

The result of an examination of the output power of the 1.06 pulse as a function of the total output power integrated over both the 1.06 pulse and the 1.12 micron pulse is presented in Figure 1. For comparison purposes we have also plotted the general form of the output power results reported for polarization preserving fibers [1]. Note that in the present instance the output power at 1.06 microns decreases precipitously on achieving a total continuous output power of 1.5 watts. A slow scanning of the input power in the vicinity of the this power can result in hysterisis loops also indicated in Figure 1.

Further examining this effect, we measured the extent of chirping about 1.06 microns,and the total output power in the SRS pulse as a function of the total output power. This data is presented in Figure 2. Note the precipitous increase in both the extent of the chirp and the SRS power. These results were readily observed in fibers of widely different lengths ,(100m, 300m and 400 m) , and index profiles (Owen-Corning 1521 step index and 1524 triangular index).

Theoretical Discussion

A complete and quantitative description of the nonlinear pulse propagation in the presence of SRS and self phase modulation is quite complicated and has yet to be performed [5]. The bistability reported here presents an opportunity to gain insight into the mechanisms surrounding the onset of SRS. Our present objective is to delineate a possible mechanism for bistability and examine its feasibility. The relationship governing the power in the SRS pulse, P_s, has the form:

$$P_s\,(t,L) \;=\; P_s\,(t,0)\,\exp\,[G_oL] \qquad (1)$$

The gain factor G is given by :

$$G_0 \;=\; \frac{g_o\,P_o\,l_w}{A_{eff}} \qquad (2)$$

where g_o is the peak Raman gain coefficient, A_{eff} is the effective area, P_o is the peak pump power, and l_w is the effective walk off length [5].

The magnitude of the chirp, $\Delta\omega_{max}$, is related to the maximum optically induced rate of change in index . If, for instance, the index change responds nearly instantaneously to a symmetric pump pulse but decays in a time on the order of the pump pulse width, then the maximum chirp, being derived from the turning points of the pulse, will be generated to the longer wavelength side of the spectrum. If the induced index change exceeds the critical value for self focusing, the beam can collapse at a point within the pump pulse and result in an increased rate of index change and moving focii that yield a discontinuous increase in the chirp the magnitude of which is given by [6]:

$$\Delta\omega_{max} = -\left[\frac{\partial\phi}{\partial t}\right] = -\left[\frac{\omega_o}{C}\right]\left[\frac{1}{V_p} - \frac{1}{V}\right]\Delta n_{max} \qquad (3)$$

The associated beam collapse would also result in a discontinuous increase in the SRS intensity.

To our knowledge , transient self focusing, has yet to be reported in optical fibers. It is not easily ruled out a priori and is intuitively appealing as working hypothesis that marshalls the qualitative features of our data.

One may examine the feasibility of a transient self focusing mechanism by estimating the value of the parameters governing the optically induced index change that results in a total index change equal to or exceeding the threshold value for focii formation. The critical power, P_{cr}, for the onset of optically induced focii is estimated to be $\frac{(1.22\lambda)^2 c}{128\ n_2}$ [7] where λ and c are vacuum values and n_2 is the familiar nonlinear index. The critical index change can be computed from the relation, $\Delta n_{cr} = n_2 \mid E_{cr} \mid^2$ where the critical electric field is related to the critical power through a knowledge of the linear impedance. We calculated $\Delta n_{cr} = 4.37\text{x}10^{-4}$ for a circularly polarized beam. The actual index change induced by the optical pulse, $\Delta\ n$, can be estimated by assuming that the net rate of change of the index is equal to the rate of increase of the dynamic index due to optical pumping minus the rate of decrease due to relaxation processes. To first order the phenomenological model takes the form:

$$\frac{\partial\Delta n}{\partial t} = \frac{1}{\tau_r}\Delta n_o - \frac{1}{\tau}\Delta n \qquad (4)$$

where Δn_o is the forcing function.

Solving for, Δn, yields :

$\Delta n(t) =$

$$\frac{1}{\tau_r}\int_{-\infty}^{t} \Delta n_o(|\ E(\eta)\ |^2) exp\{\frac{-(t-\eta)}{\tau}\} d\eta \qquad (5)$$

Setting $\Delta n_0(|E(\eta)\ |^2) = n_2|E|^2$, $n_2 = 1.1\text{x}10^{-13}$ esu and using a gaussian approximation to the pump pulse with $FWHM = 90_{PS}$ and the peak value $E^2 = 4.84\text{x}10^{-14}$, $\frac{V^2}{m^2}$ determined by the measured SRS onset power, we obtained values of τ and τ_r for which the maximum value of Δn equals the critical value. These values are plotted in Figure 3 (solid line).

To gain further insight into the dynamics of the induced index change, we plot the index as a function of time for $\tau_r = 1.83\text{x}10^{-15} sec$ and $\tau = 75_{PS}$, assuming the gaussian pump pulse measured at the onset of SRS. These particular values of τ and τ_r are within the range of values found in literature for nonlinear indices in bulk SiO_2 [8]. As shown in Figure 4 the index change attains a maximum value equal to Δn_{cr} at a time t_d after the peak of the pump. In Figure 3 we have also plotted the values of t_d for the threshold pump intensity corresponding to each pair of τ and τ_r that yield a maximum value of Δn equal to the critical value. From this plot one may estimate where self focusing begins within the pulse.

The moving focii concept of transient self focusing [6] provides an interesting way of viewing the onset of SRS. Self focusing is associated with a very rapid index change that tends to precipitate strongly chirped SRS . In one extreme the focii may be quickly dissipated by the generation of SRS or higher order mode generation, thus being incipient or virtual. In such cases bistability may not be observed. In the other extreme the focii may receive positive feedback through the SRS process. For example, if the SRS pulse forms at the trailing edge of the pump pulse and propagates at a higher group velocity

net optical energy will be transferred forward and will thereby advance the point of peak optical power . The focii , which advances faster than the pump velocity begins to walk through the pump pulse into regions of higher optical flux and is reinforced. This process will self terminate as the SRS pulse walks off the pump pulse. This purely travelling wave phenomenon provides a bistability mechanism distinctly different from the standing wave varieties found in the literature [10].

Conclusions

Optical fibers exhibit bistable behavior when pumped by high power pulses. The bistability is allied with the onset of SRS. Discontinuous changes in chirp and SRS production strongly indicate the presence of a mechanism which involves a discontinuous increase in the index induced by large optical field intensities. Our analysis indicates that transient self focusing is a likely mechanism. Further experimental and theoretical investigation along these lines should provide a better understanding of chirping and SRS in optical fibers. We intend to continue these investigations.

Acknowledgements:

The authors gratefully acknowledge stimulating discussions with J. Heritage, R. Stolen and R. R. Alfano. We also thank Corning Glass Works for their generous gifts of single mode fiber. This work was supported by grants from the Air Force Office of Scientific Research (Grant # AFOSR-84- 0377) and the National Science Foundation (Grant # NSFECS-8404495)

References

1. J. Heritage, A. M. Weiner, and R. N. Thompson, Proc. of the Topical Meeting on Ultrafast Phenomena, Aspen '86.
2. D. Grischkowsky, and A. C. Balant, Appl. Phys. Lett. 41(1), 1-3 July 86.
3. D. Schadt, B. Jaskorzynska and U. Osterberg, JOSA:B, to be published.
4. N. Gitkind, and A. P. DeFonzo, OFC/IOOC '87, Accepted for publication.
5. R. H. Stolen and A. M. Johnson, IEEE Journ. of Quantm. Electrncs., QE-22, 2154-2160 (1986).
6. Y. R. Shen, The Principles of NonLinear Optics, Chap 17, Wiley-Int (1984).
7. R. Y. Chiao et. al. Phys. Rev. Lett., 15, 479-482 (1964).
8. D. Heiman, R. W. Hellwarth and D. S. Hamilton, Journ. Non-Crystl. Solids , 34, 63-79 (1979).
9. D. H. Austin, Picosecond Nonlinear Optics, Ultrashort Light Pulses,ed. S. L. Shapiro, Springer Verlag, Berlin (1977).
10. Hyatt Gibbs, Optical Bistability, Academic Press, Orlando, (1985).
11. R. P. Feyman, F. L. Vernon and R. W. Hellwarth, J. Appl. Phys. 28, 49 (1957).

Figures

Figure 1. Pump power out versus total (pump +Raman) power out in 300 meter single mode fiber. Solid and dashed lines are our data. Dotted line shows form of data reported for polarization preserving fiber [1].

Figure 2. Chirp of the pump pulse and the Raman power output as a function of the total power in a 300 meter long single mode fiber

Figure 3. The two characteristic times,τ and τ_r for which the induced index change, Δn, attains the critical value for self-focusing at an input power of 1.4 W (solid line). The dotted line is the time delay , τ_d , between the pump pulse peak and the time at which the critical index is reached.

Figure 4. Theoretically calculated non linear index change as a function of time for $\tau = 75psec$ and $\tau_r = 1.83\text{x}10^{-15}$ for Pav = 1.4 W (solid line). Also shown is the pump pulse as a function of time, $FWHM = 90psec$ (dotted line). Note that the index reaches a maximum value just equal to the critical value for self focusing, $\Delta n = 4.37\text{x}10^{-4}$ at a time $t_d = 38.6psec$ after the peak of the pulse.

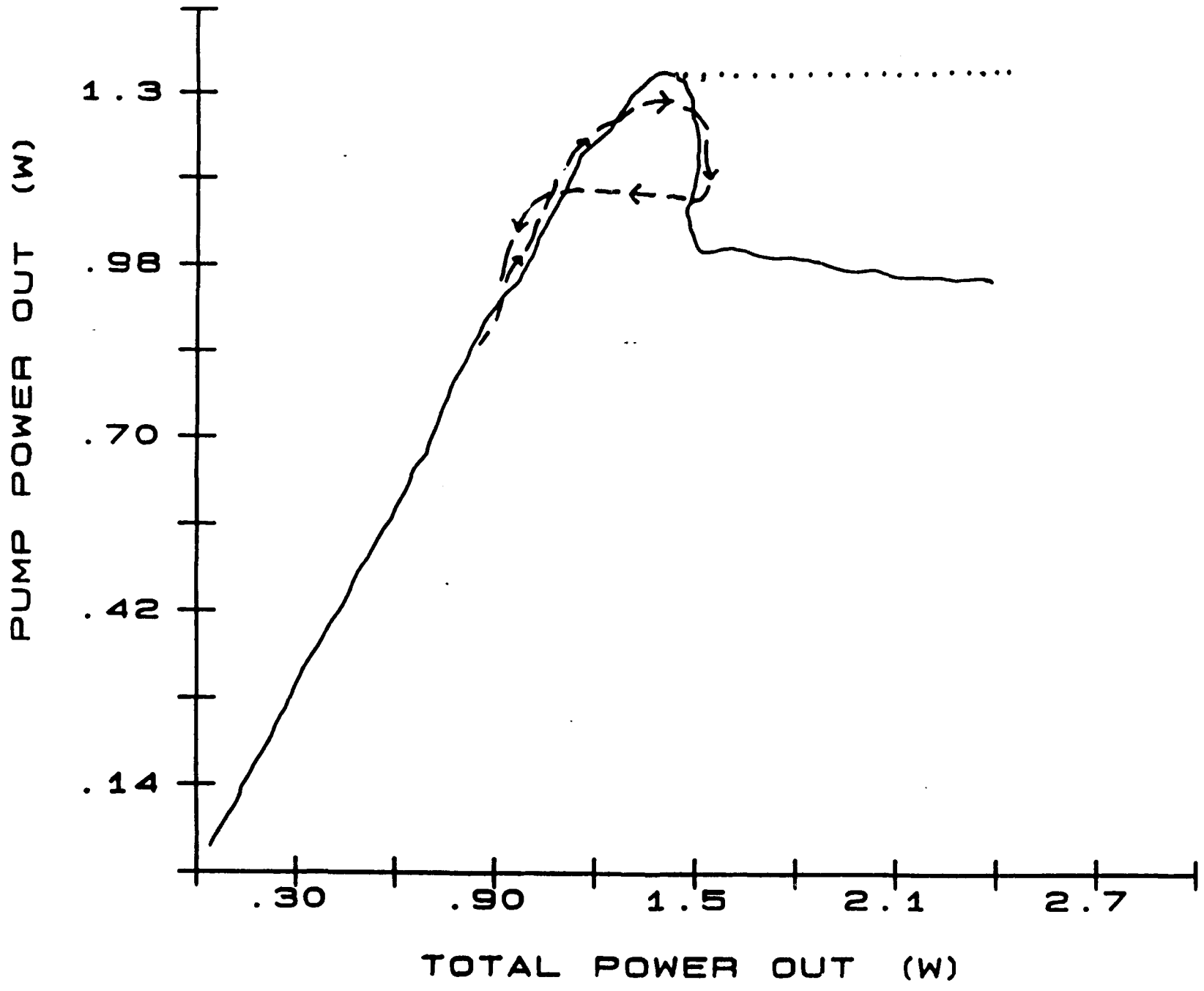
PUMP POWER OUT (W)
1.3
.98
.70
.42
.14
.30
.90
1.5
2.1
2.7
TOTAL POWER OUT (W)

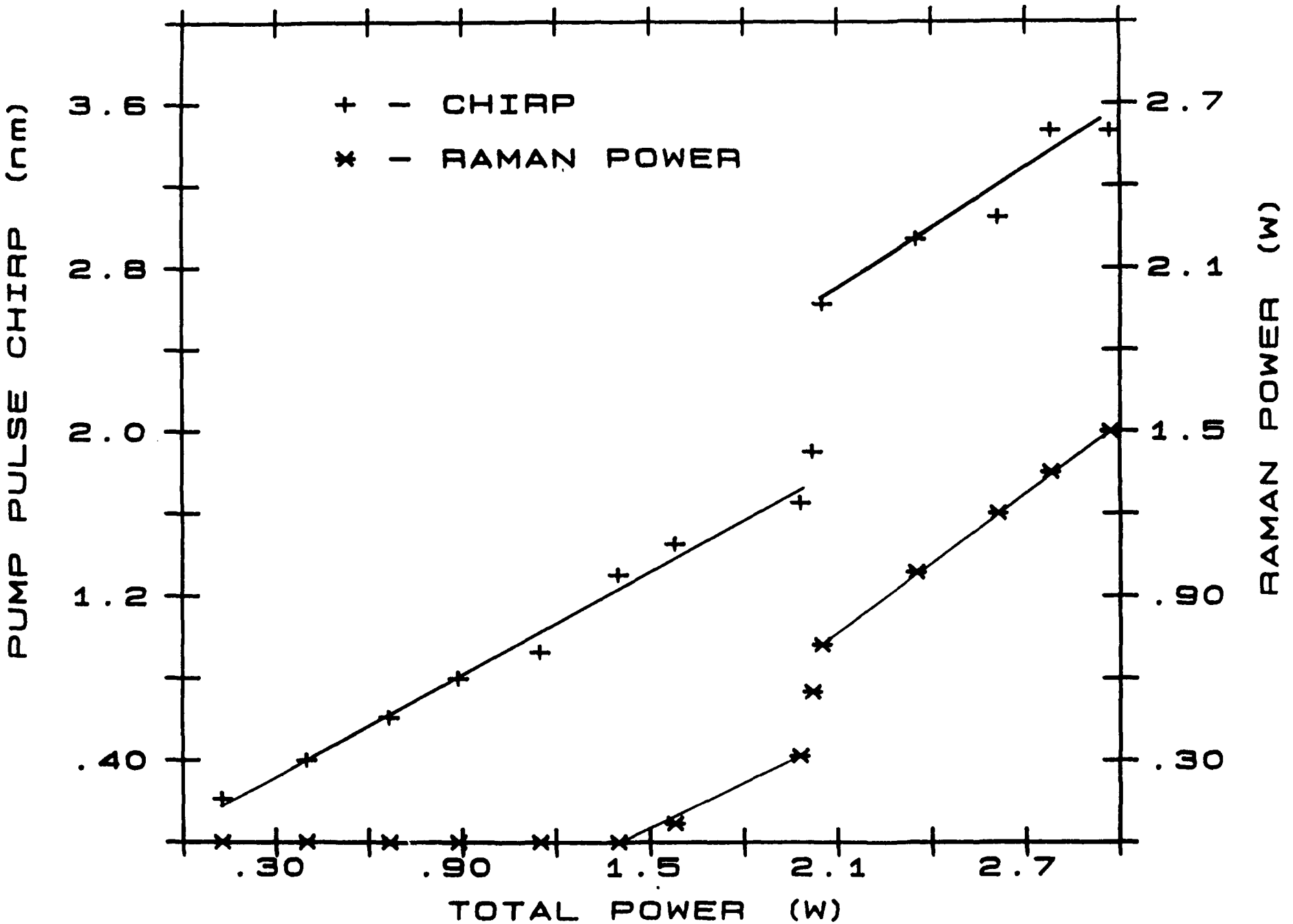
+ - CHIRP
* - RAMAN POWER
PUMP PULSE CHIRP (nm)
3.6
2.8
2.0
1.2
.40
RAMAN POWER (W)
2.7
2.1
1.5
.90
.30
.30
.90
1.5
2.1
2.7
TOTAL POWER (W)

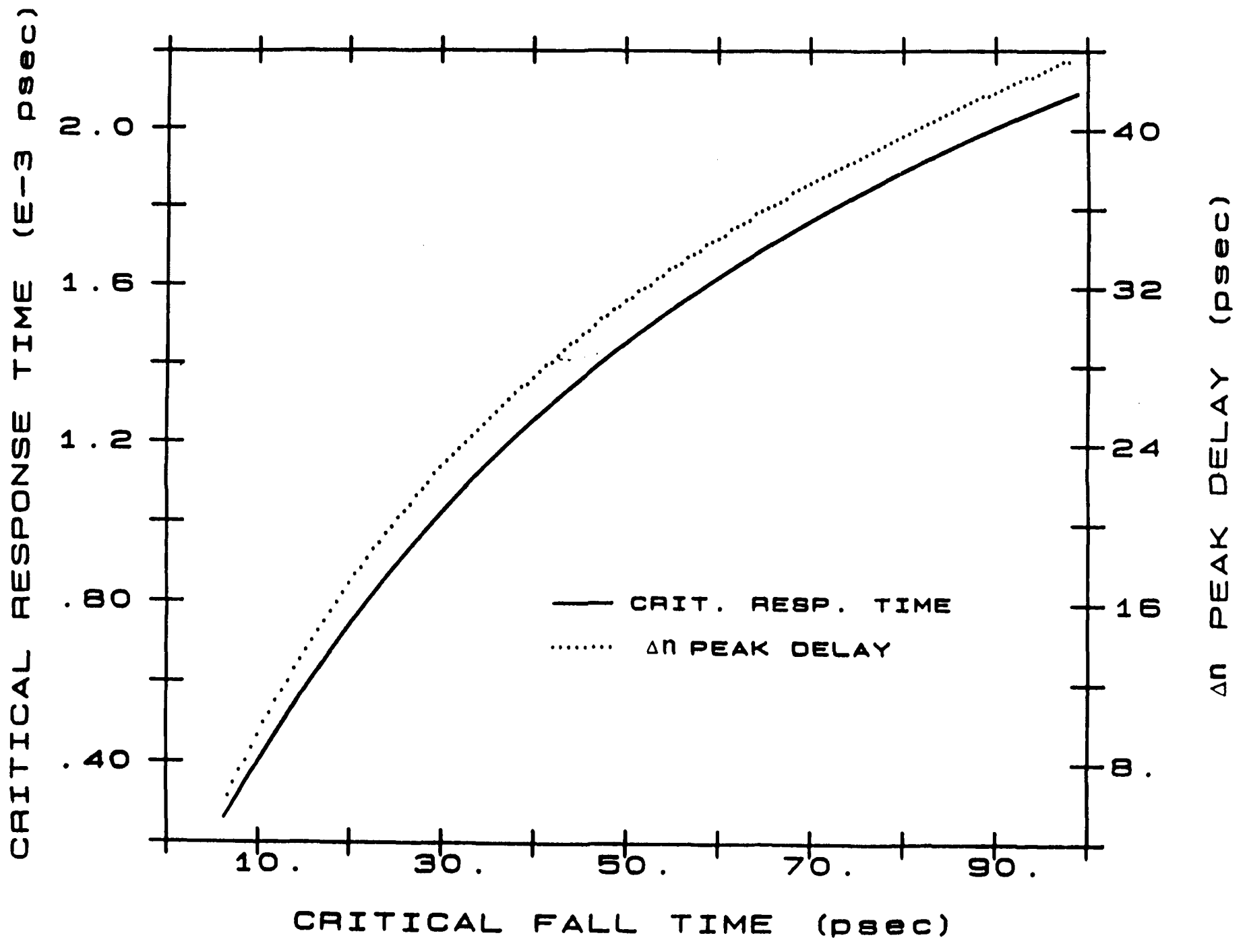
CRITICAL RESPONSE TIME (E-3 psec)
2.0
1.6
1.2
.80
.40
40
32
24
16
8.
Δn PEAK DELAY (psec)
CRIT. RESP. TIME
Δn PEAK DELAY
10.
30.
50.
70.
90.
CRITICAL FALL TIME (psec)

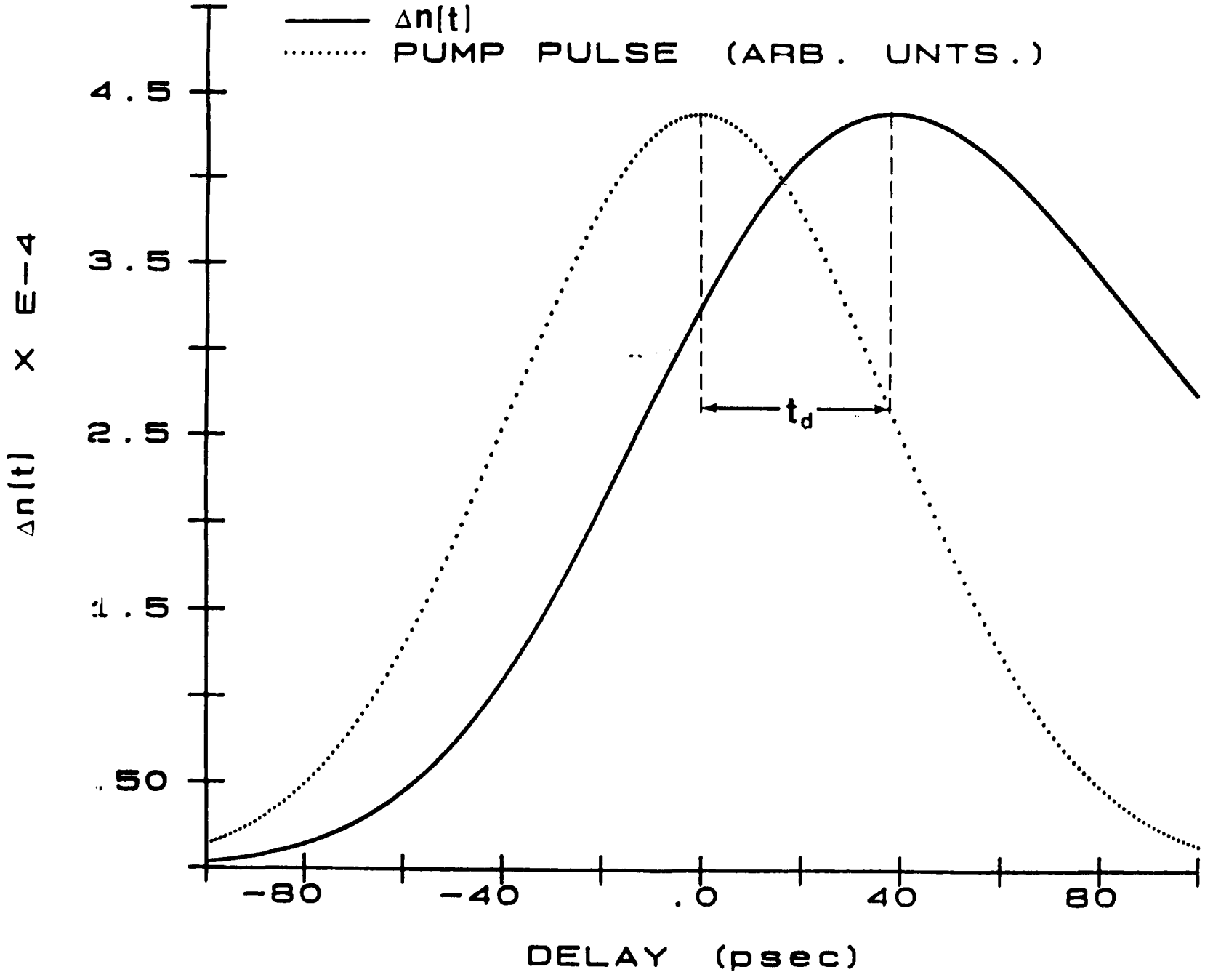
Δn(t)
PUMP PULSE (ARB. UNTS.)
4.5
3.5
2.5
1.5
.50
Δn(t) X E-4
t_d
-80
-40
.0
40
80
DELAY (psec)

To be subm. Optics Comm.

Transient Stimulated Raman Scattering in ordinary single-mode fiber

Neil Bitkind and M. F. DeFonzo

Dept. of Electrical and Computer Engineering, Univ. of Massachusetts Amherst, MA 01003

1 Introduction

The growing application of frequency chirped pulses due to self Phase Modulation (SPM) in optical fibers has generated renewed interest in the study of Stimulated Raman Scattering (SRS), and its effect on pump pulse chirping. Much of the recent experimental work has concentrated on polarization preserving fibers pumped by visible light [1,2,3,4] or Nd:YAG [5] radiation. Others have studied "ordinary" fibers pumped in the visible [4,6] and by Nd:YAG [7]. Very large chirps have been reported for SRS pulses [1] and attention is being increasingly directed toward their possible use. In this paper we report the results of an experimental study of the generation of SRS pulses pumped by circularly polarized Nd:YAG laser pulses at 1.06 um (peak throughput powers up to 420 Watts) launched into an ordinary germanium doped single mode optical fiber (Owens Corning 1521, core diameter = 8.7 microns).

When SRS is pumped by short enough pulses in a long enough fiber the Raman radiation will separate from the pump radiation due to their different velocities in the fiber. The SRS pulses observed to date [2,5] have been down-shifted in frequency by 440 cm-1 corresponding to the broad Raman band in fused silica. We also observe a pulse corresponding to a strong conversion to the two phonon band shifted by 880 cm-1. In addition we report the measurement of absolute pump pulse propagation delays and how this information may be used to determine the origin, along the fiber, of the Raman pulse.

The existence of transient stokes/anti-stokes pairs about 1.06 microns in a single mode fiber have been conjectured but not reported in the literature. Stokes/anti-stokes generation does not readily occur in bulk SiO2 because the phase velocities do not satisfy the phase matching conditions for four wave mixing. We report here the first observation of strong SRS stokes/anti-stokes generation in an optical fibers.

BEST AVAILABLE COPY

2 Experimental

2.1 Setup

The experimental set up is schematically shown in figure 1. The optical components are identical to those we have described in detail elsewhere [7]. One hundred picosecond pulses from a mode-locked (100 MHz repetition rate) Nd:YAG laser (max. peak power = 800 W) are circularly polarized and coupled to an optical fiber. Measurements yielded a coupling efficiencies between 55 and 65 percent. The pump pulse propagates along the fiber generating a

strong chirp (due to SPM) and various SRS pulses. Upon exiting the fiber and passing a quarter wave plate and an analyzer the beam is initially split. One beam excites a high speed InGaAs photodetector (rise time = 35 ps). The detector output is temporally analyzed with a 5 GHz sampling head (rise time =25 picoseconds) and displayed on a Tektronix 7404 oscilloscope. Another beam is directed into a grating spectrometer (Spex HR320) outfitted with a silicon photodiode array, the output of which is simultaneously displayed. The average power over all wavelengths exiting the fiber is monitored and further passed through a holographic grating pair in the Littrow configuration for spatial analysis, additional spectral analysis, and an eventual monitoring of the pump output power.

2.2. Results

2.2.1 Spectral

We found that we could selectively excite groups of SRS lines by adjusting the coupling to the fiber. At optimum coupling we always observed the 440 cm-1 down-shifted line ($\lambda s2$) along with a two phonon line down-shifted by 880 cm-1 ($\lambda s3$). Figure 2(a) shows the excited spectra at this coupling condition for four input powers. The absence of the second order SRS spectrum for 3.0 and 1.9 Watts is due to a lack of sensitivity of the diode array. The evolution of the first Raman line is characterized by the appearance of a double hump for the case of high Raman conversions. This has been previously observed in both ordinary and polarization preserving fibers [3,4]. Note also the broadening, due to SPM, of the pump spectrum with increasing power, and its marked asymmetry. At high input powers, more stokes lines are induced, however the observation of these lines beyond the second order was also prohibited by the response of our silicon photodiode array.

When the fiber is miscoupled (coupling efficiencies no greater than 20%) we observe a nearer stokes pulse down-shifted by 140 cm-1 ($\lambda s1$) its anti-stokes counterpart ($\lambda a1$), and $\lambda s2$ (Figure 2(b)). The two phonon pulse is not observed in this case.

2.2.2 Temporal

Figure 3 is a collection of oscilloscope traces which corresponds to measurements performed on a 400 meter fiber. The output pump pulse is on the right. As the input power is increased we see the appearance of the first order Raman pulse ($\lambda s2$) leading the pump pulse. A further increase in power yields the observation of $\lambda s3$. Note that in the presence of strong Raman conversion, the pump pulse acquires sloped edges and is in fact shorter than at the input despite the temporal spreading that SPM and dispersion impart upon it [8]. Note also the shoulder on the output pump pulse. This is indicative of scattering to $\lambda s1$ which was always present for large throughout peak powers. A monitor from the fiber input beam was focused onto the same fast photodiode and the position of its peak is indicated by the [illegible] of the trace left. Its presence provides an absolute indication of the change in time of arrival of the pump pulse as the input power [illegible] Raman conversion changes. Figure 4 is a plot of the arrival [illegible] the pump pulse versus input power. Note that higher input powers result in a larger delay, and hence a slower travelling pump pulse.

BEST AVAILABLE COPY

The rather large relative errors are due to small changes in coupling efficiency from run to run. The data indicates that greater coupling results in a steeper line shifted to lower powers.

When the coupling is adjusted to induce the λ_{s1} and λ_{a1} SRS (this was done by translating the fiber end in the plane perpendicular to the beam axis) the output spectrum changes continuously but is bound by two extreme cases. In one case we see the most coupling to the anti-stokes line. It appears in a well defined "doughnut" pattern having an angular distribution spanning 32 to 114 mrad (interior to the fiber). This coupling produces the corresponding stokes line having a comparable strength. The other condition maximizes coupling to the stokes wavelength. In this condition we see weak coupling to the anti-stokes wavelength. Large conversions to λ_{s2} and more up-shifted radiation (having a central spatial null) continuously distributed between the pump wavelength and the anti-Stokes wavelength. This may be further anti-Stokes creation due to the broadband stokes radiation observed under these coupling conditions. Figures 5 and 6b correspond to this coupling condition. In figure 5 there are three distinguishable output pulses. The leading pulse (on right) corresponds to the Nd:YAG pump pulse. The middle pulse is the SRS pulse at 1.08 microns arriving 135 psec ahead of the pump pulse. The leading pulse is again the 440 cm-1 shifted Raman pulse at 1.12 microns and leads the pump pulse by 435 psec. The anti-stokes pulse contains higher frequency components and would hence lag the pump pulse. Due to a low level of conversion to this frequency and ringing in the trace, the pulse is not visible.

3. Theoretical

3.1 Temporal Dependence

The analysis of the temporal walk off due to fiber material dispersion presented here is based on the analysis recently presented in the literature [2]. Stolen has proposed a simple intuitive model for pulse walkoff and its relation to SRS gain. Basically, the SRS pulse "walks through" the pump pulse due to the differential in group velocity. Developing a general theoretical picture of such phenomena is obviously very difficult. Numerical simulations which indicate the complexity of the processes have been performed for particular cases [3]. We approach the problem experimentally by isolating qualitatively different phenomena and using relatively simple intuitive concepts to organize and quantify the salient features of the data.

First we examine the walk-off rates of the various pulses. Since the various SRS pulses are well defined in the time domain, rate of walk-off may be estimated in lowest order through knowledge of the material dispersion D(lambda) [10] for the "center" wavelengths of the Raman and pump pulses. From [2]:

$$\Delta t = \frac{L\,D(\lambda)\,\Delta\nu}{c\,\nu} \qquad (1)$$

where L is the fiber length, nu is the average frequency, and del nu

BEST AVAILABLE COPY

is the frequency separation between the pump and stokes lines. Also we may define, after Stolen [2], a walkoff length, lw, to be the distance it takes for a longer wavelength Raman pulse to pass through a slower, copropagating pump pulse of width T. For a 100 psec Nd:YAG pump pulse and its 440 cm-1 down shifted Raman line this length is 70 m. Distance along the fiber may be normalized by this parameter. Given the delay between the pump and stokes lines at the fiber output and the calculated walk-off rate the origin of the SRS pulse can be estimated. With the additional knowledge of the absolute delay of the pump pulse one can more accurately calculate the point of Raman pulse origin. Figure 6 is a plot of this calculation. In our case, knowledge of the absolute delay corrects the calculation by as much as a factor of two in distance from the fiber origin. The longer the fiber and the higher the conversion, the more this correction becomes necessary.

3.2 Anti-Stokes generation

We attribute the anti-stokes generation to a parametric process [11]. The following phase matching condition must be satisfied:

$$kp = ks + kas \qquad (2)$$

For an isotropic medium having normal dispersion this condition can only be satisfied when kas and ks are not codirectional with kp (i.e. |k| = nw/c). Hence the theory of anti-stokes scattering predicts the generation of a cone like sheath of radiation emanating from the interaction region (where phase matching is satisfied). For plane wave mixing, the cone half-angle, beta, is given by:

$$\text{beta} = \frac{1}{n}\sqrt{\frac{\Delta\omega}{\omega}} \qquad (3)$$

The above relation yields beta = 16.3 mrad (.93 degrees). In the fiber however the observed fundamental mode in which the pump line and all down-shifted lines were observed in is angularly distributed over about 75 mrads corresponding to a fiber N.A. of 0.11 . Due to this distribution of k vectors in the mode, it is necessary to integrate over all phase matching conditions that can exist in the fiber. Also, if self focussing is occurring in the fiber (this is consistent with the instability we observe in the fiber [7]), this will broaden the observed distribution [12]. A complete analysis of this phenomenon is beyond the scope of this paper.

4 Discussion

In the absence of pump depletion the stokes radiation only [illegible] the fiber with the leading edge of the pump pulse will see the gain. Since the pump pulse is about 2 cm long in glass, the [illegible] between the stokes line and the pump line begins early in the [illegible] and much of the interaction would be expected to have taken place [illegible] the first walkoff length. With pump depletion, the peak [illegible] stokes pulse will develop from earlier portions of the pump pulse [illegible] earlier in the fiber (Stolen has also noted this trend). For the case of self-focussing the Raman gain (being proportional to [illegible] density [2]) is further increased, presumably placing the origin [illegible]

BEST AVAILABLE COPY

the Raman pulse yet earlier. On the other hand, the temporal broadening of the pump pulse due to SPM and group velocity dispersion will tend to push the creation point of the SRS pulses further into the fiber as it will simply take longer to walk through the widened pump. The data indicates that for small Raman conversions, the SRS pulse is created between two and three walkoff lengths into the fiber and that for large conversions the creation region is indeed earlier in the fiber and constant at about 1.8 walkoff lengths from the input. Of course for high conversions, the situation is further complicated by the presence of higher order scattering. As more pulses are being treated (e.g. λ_{s3}) the interpretation of the temporal data becomes more difficult. Then we may have to take into account the extent to which the spectrum of the first order pulse, and hence its velocity, is affected by its interaction with the second order pulse. The spectral and temporal data indicates the complexity of this interaction.

As indicated, the pump-SRS interaction destroys the spectral symmetry, created by SPM, of the pump pulse. SPM creates wavelength sidebands of a value proportional to the derivative of the pulse power envelope. Consequently, long wavelengths appear at the leading side of the pulse and short wavelengths on the lagging side. Chirps on the order of 50 cm-1 (4.2 nm) are routinely observed on the pump pulse. (after 90cm fiber propagation) whereas the 1.12 micron Raman line is about 440 cm-1 from 1.06 microns. Furthermore, the material dispersion has a nearly linear dependence on frequency in the vicinity of these wavelengths [8]. These considerations suggest that the SRS pulse should walk through the pump pulse at least twelve times faster (4 ps/5) than the pump pulse can spread out. The qualitative result is that the SRS pulse eats away the leading portion of the pump pulse thereby stripping it of its long wavelength components. Figure 4 depicts the consequences of this interaction. This effect is seen in the chirped pump pulse in figure 2(a) (the case of optimal coupling). We have observed an opposite sense of spectral skew when the λ_{s1} Raman conversion is high (figure 3(b)). This line is not frequency shifted as far from the pump, hence its walkoff velocity is slower, increasing its interaction with the central portion of the pump pulse. The anti-stokes line travels at a group velocity which is less than that of the pump pulse so it would tend to 'eat' at the lagging side of the pump.

Conclusion

A total of three distinct SRS pulses have been observed. Two (λ_{s2} and λ_{s3}) originate from the well known Raman band in fused silica while the third, λ_{s1} originates from a previously unreported Raman band centered at 1.35 cm-1. The experimental and theoretical results demonstrate that the SRS stokes pulses originate in the trailing edge of the pump pulse and experience gain by walking through the pulse in accordance with the models presented earlier [1,2,3]. When only the stokes radiation is present this results in an eating away of the longer wavelength chirped components of the pump pulse as was previously reported. For the nearer stokes pulse λ_{s1} the walkoff rate is slower thereby increasing its interaction with the central portion of the pump pulse. The origin of the first order Raman pulse can be

BEST AVAILABLE COPY

estimated through knowledge of the pulse delays and velocity differences. This was done for the case of optimal coupling to λ 5... The observed SRS anti-stokes line is generated parametrically through the interaction of the near stokes pulse and the pump pulse. Its angular distribution is characterized by a large central null.

Acknowledgments

The authors gratefully acknowledge Corning Glass Works for their generous gift of single mode fiber. Thanks also to Dan Vassilovski for his determined and helpful aid in these experiments. This work was supported by the Air Force Office of Scientific Research (Grant # 84-0377) and the National Science Foundation (Grant # 8404495).

References

1. A.M. Johnson, R.H. Stolen and W.M. Simpson, Proc. of the Topical Meeting on Ultrafast Phenomena, Snowmass, CO. 1986.

2. R.H. Stolen and A.M. Johnson, IEEE J. of Quantum Electron., QE-22, 2194-2160, 1986.

3. P. Stenersen and R.K. Jain, Optics Comm., 51, 121-126, 1984.

4. R.H. Stolen, C. Lee and R.K. Jain, J. Opt. Soc. Am. B, 1, 652-657, 1984.

5. A.M. Weiner, J.P. Heritage and R.H. Stolen, CLEO '86 Technical Digest, p. 246.

6. E. Valk, W. Hodel and H.P. Weber, Optics Comm., 54, 363-368, 1985.

7. A.P. Detonzo and N. Bitkind, Submitted to Optics Letters.

8. D. Grischkowsky and A.C. Balant, Appl. Phys. Lett., 41, 1-3, 1982.

9. D. Schadt, B. Jaskorzynska and U. Osterberg, to be published.

10. D. Blood, Appl. Optics, 10, 2442-2443, 1971.

11. A. Yariv, Quantum Electronics, 2nd Ed., Chap 18, Wiley 1975.

12. T. Shimoda, Japanese J. Appl. Phys., 5, 86-92, 1966.

FIGURE CAPTIONS

Figure 1. Experimental layout.

Figure 2. Output spectrum from a 400 meter single mode fiber pumped by a 100 psec Nd:YAG pulse. a) Spectrum at optimal coupling at four peak throughput powers. b) Spectrum for the anti-stokes coupling condition where conversion to the anti-stokes band is maximized.

Figure 3. Output pulses from a 400 meter single mode fiber pumped by various powers of a 100 psec Nd:YAG pulse. Trace is from a 5 ps sampling head (risetime = 35 psec) and a InGaAs photodetector (risetime = 35 psec). Pulse on left is sampled from the input beam and provides an absolute reference for the delay of the exiting pulses on the right.

Figure 4. Peak throughput power versus the delay of the output pump pulse relative to its below Raman threshold arrival time.

Figure 5. Typical output trace for the coupling condition which maximizes conversion to the near Raman band (λs1). Same diode and sampling head as in Figure 3.

Figure 6. Calculated origin of the first order Raman pulse (λ s1) as a function of peak throughput power.

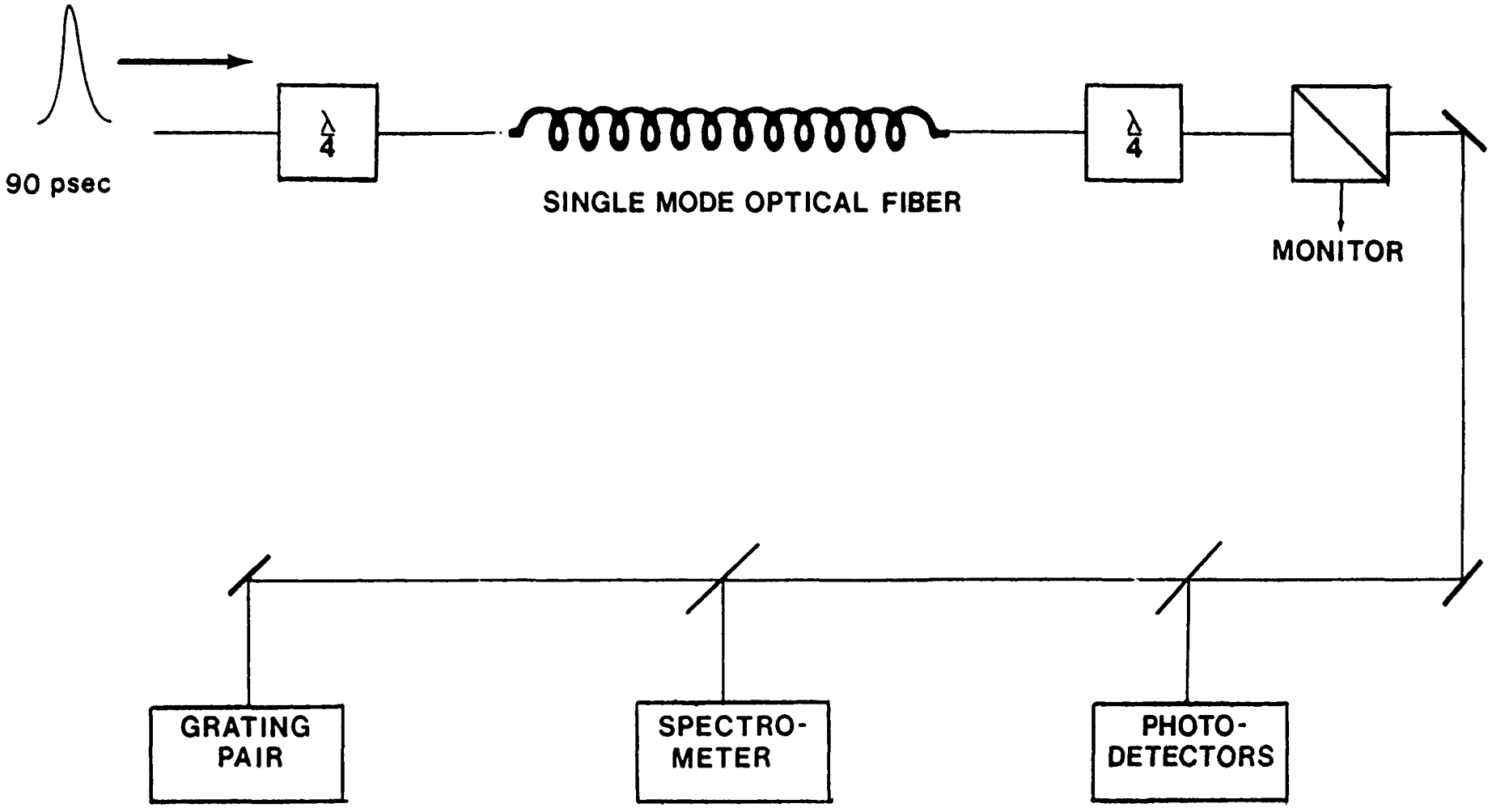
90 psec
λ/4
SINGLE MODE OPTICAL FIBER
λ/4
MONITOR
GRATING PAIR
SPECTRO-METER
PHOTO-DETECTORS

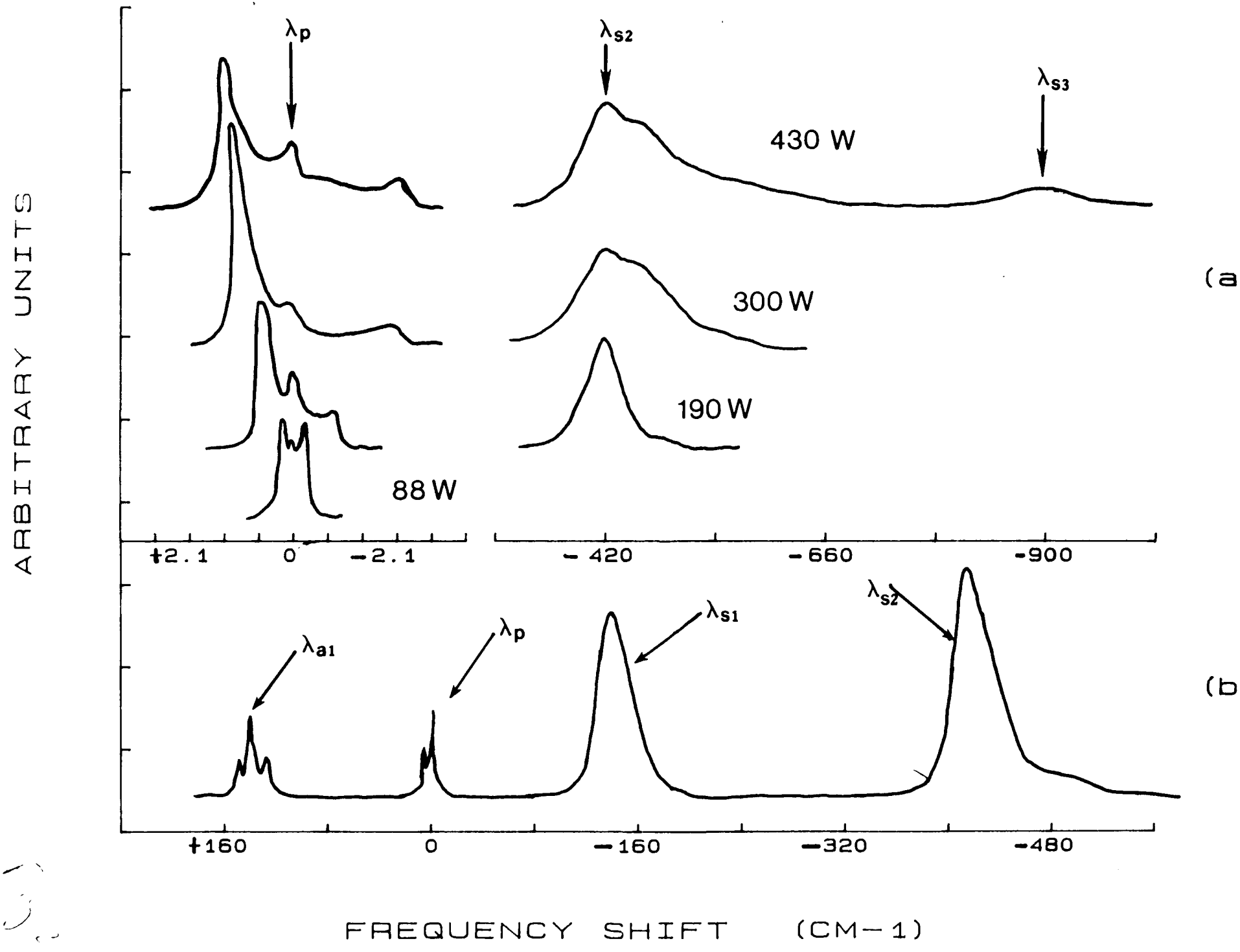
ARBITRARY UNITS
λp
λs2
λs3
430 W
300 W
190 W
88 W
+2.1
0
−2.1
−420
−660
−900
(a
λa1
λp
λs1
λs2
(b
+160
0
−160
−320
−480
FREQUENCY SHIFT (CM−1)

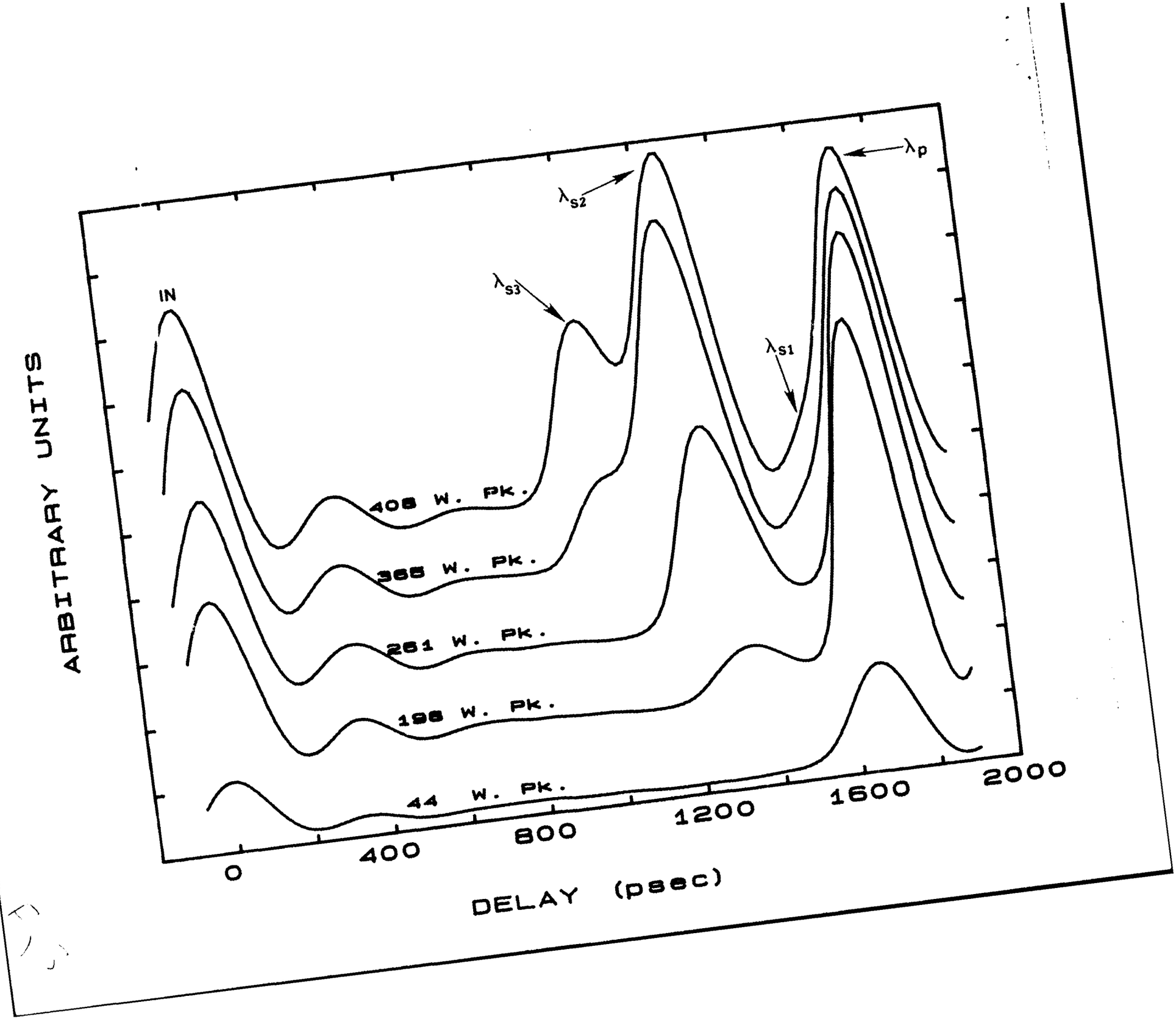
ARBITRARY UNITS
IN
λ_{s3}
λ_{s2}
λ_{s1}
λ_p
408 W. PK.
365 W. PK.
261 W. PK.
198 W. PK.
44 W. PK.
0
400
800
1200
1600
2000
DELAY (psec)

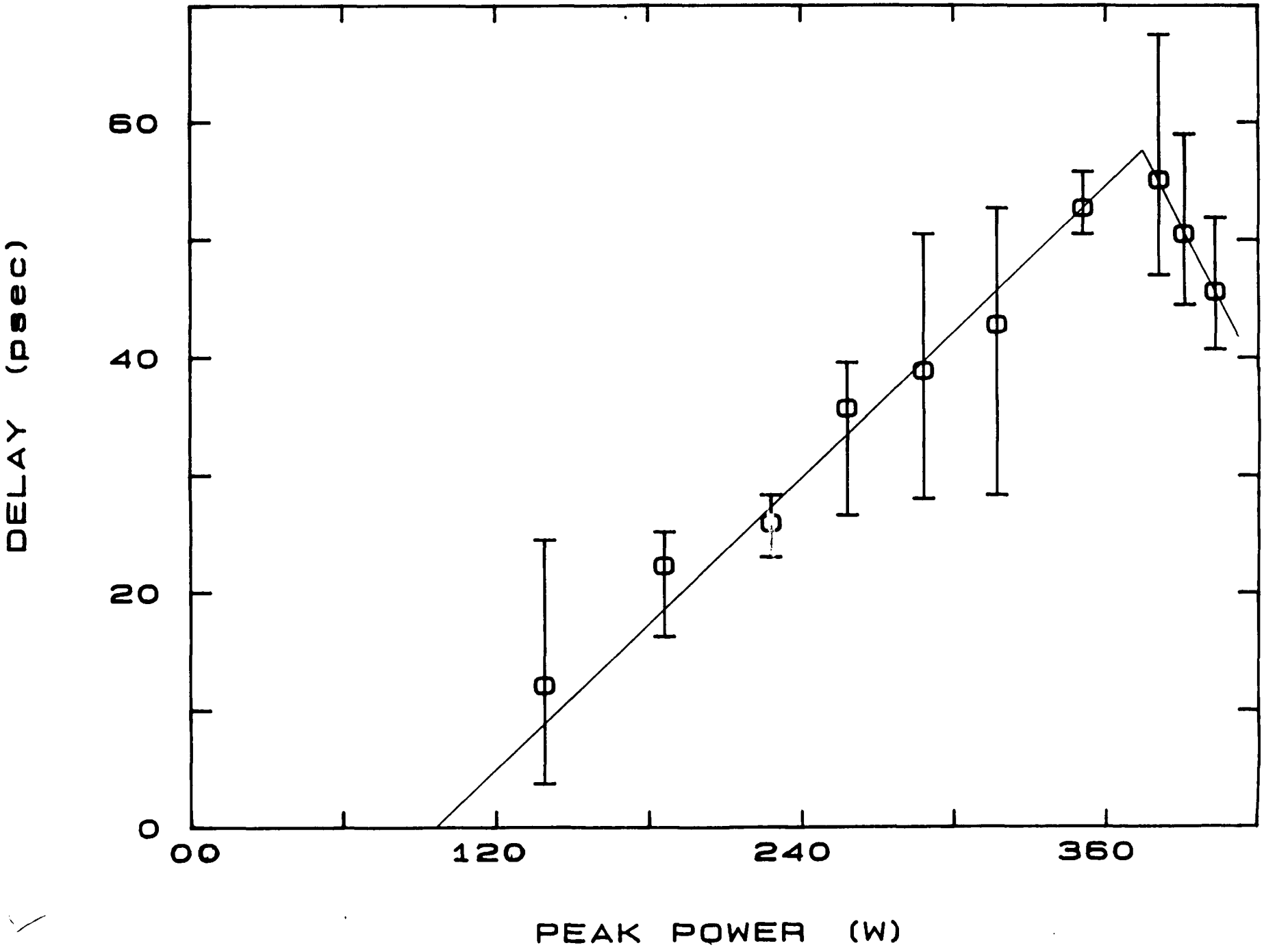
60
40
20
0
00
120
240
360
DELAY (psec)
PEAK POWER (W)

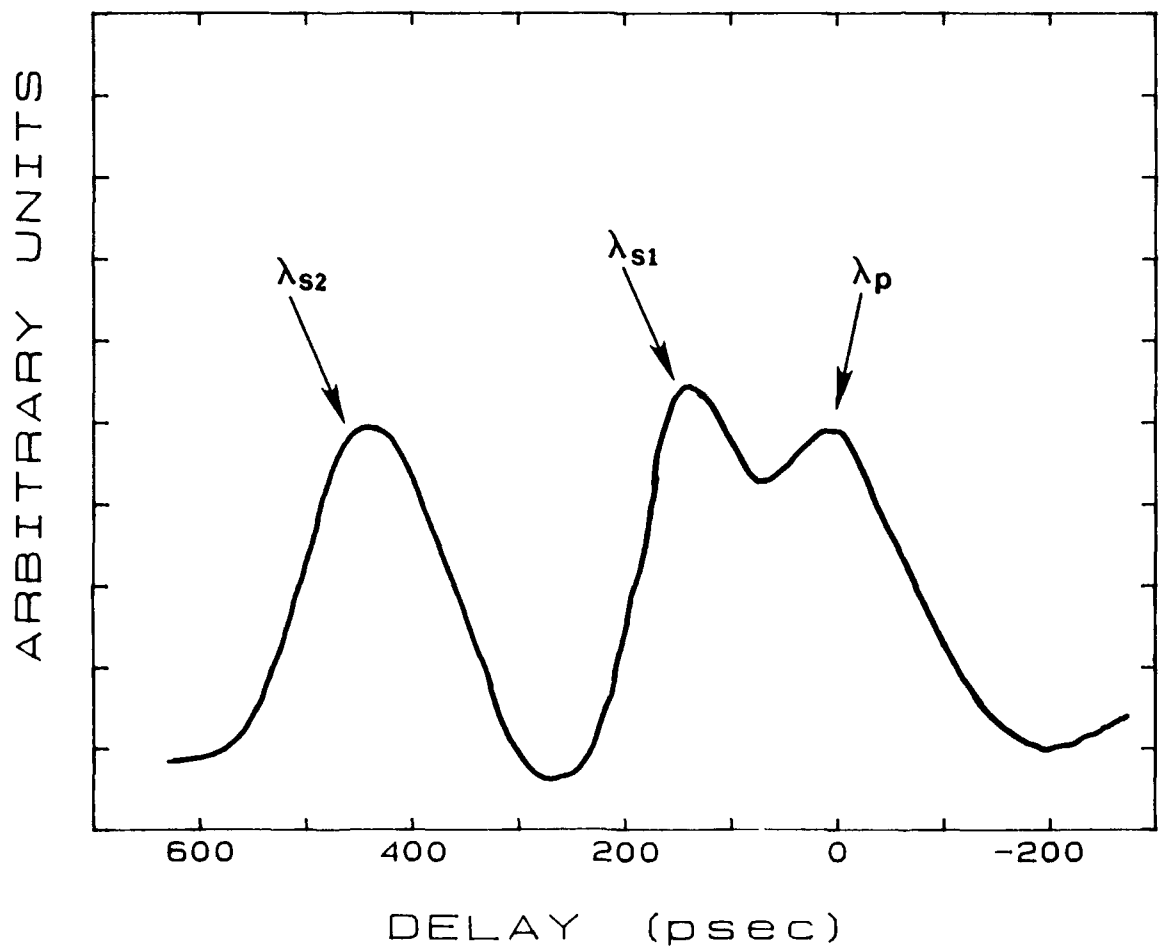
ARBITRARY UNITS
λ_{S2}
λ_{S1}
λ_p
600
400
200
0
-200
DELAY (psec)

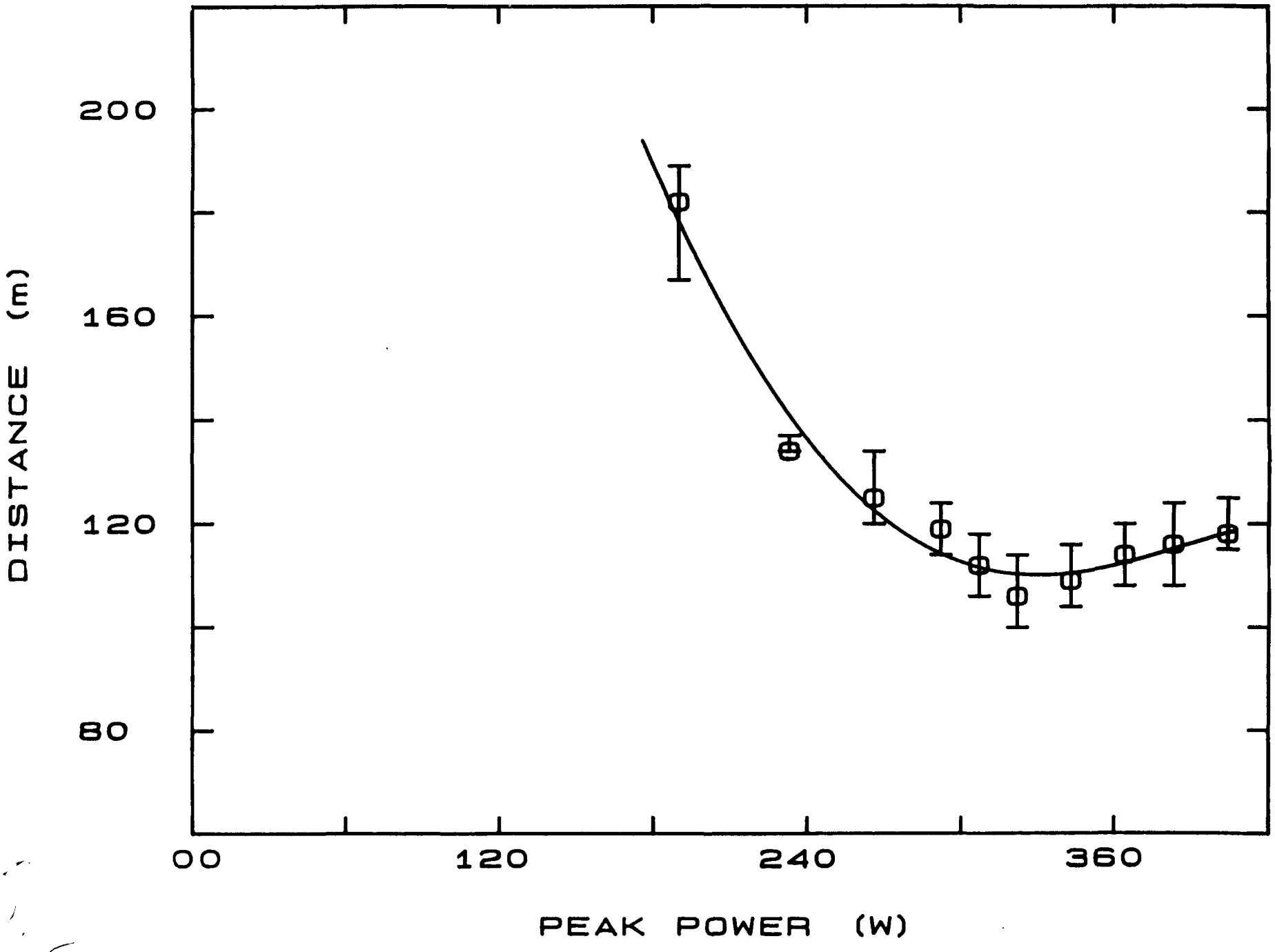
200
160
120
80
DISTANCE (m)
00
120
240
360
PEAK POWER (W)

Accepted
OFC/IOOC '87
(Rapid)

Stimulated Raman Scattering in Single Mode Optical Fibers

Neil Gitkind, Alfred P. DeFonzo

Dept. of Elect. and Comp. Engineering, University of Massachusetts

142 Marston Hall, Amherst, MA 01003

(413)545-2374.

The results of a systematic study of the propagation of high, average and peak power, circularly polarized, mode locked Nd:YAG laser pulses in 400 m and 50 m fibers is presented. The first direct observation of a stimulated Raman scattering pulse at 1082 nm, its frequency chirp and respective walkoff is presented.

Stimulated Raman Scattering in Single Mode Optical Fibers

Neil Gitkind, Alfred P. DeFonzo
Dept. of Elect. and Comp. Engineering, University of Massachusetts
142 Marston Hall, Amherst, MA 01003
(413)545-2374.

Recent interest in optical pulse compression, particularly at 1.06 μm has resulted in several experimental[1] and theoretical[2] studies of the interaction of Stimulated Raman Scattering (SRS) and Self-Phase Modulation (SPM) in polarization preserving fiber. Similar work[3] has been reported for shorter wavelengths. In this paper we shall discuss the interaction of SRS with the self-phase modulated pump pulse using non-polarization preserving fiber at throughput powers of 1 to 4.5 watts continuous. We observed for the first time, the generation of an SRS pulse at 1.082 μm which can be excited either alone or in tandem with the previously reported 1.12 μm SRS pulse. These pulses can exhibit exceptionally large spectral broadenings of 70 Å and 400 Å respectively and may present an opportunity to generate extremely short pulses at these two wavelengths.

Our measurements are made with an 85 psec, 1.06 μm pulse from an actively mode-locked Nd:YAG laser focused onto a single mode fiber (Corning 1521, 8.7 μm core diameter). The incident pulse is circularly polarized, and only this polarization component of the exiting pulse is analyzed and studied in these experiments. Both a 50 meter and a 400 meter fiber were investigated.

We present three cases. Figure 1 shows the exiting pulse and corresponding spectrum for the 50 m fiber. No Raman pulse was detected, however the slight assymetry of the SPM spectrum is indicative of nominal Raman

conversion. For the 400 m fiber, we find that there exists substantial interaction length to promote higher Raman conversions. Figure 2 shows the 1.12 μm Raman and Nd:YAG pulses as they exit the 400 m fiber. The Raman pulse leads by approximately 420 psec because of its differing group velocity. The assymetry in the Nd:YAG spectrum is indicative of strong Raman conversion. Figure 3 shows the propagation of the Raman line at 1.082 μm. This pulse leads by 185 psec and has also caused a drastic assymetry in the Nd:YAG spectrum (figure 3B at left). Also seen was an anti-stokes line centered at 1.046 μm. However conversion to this wavelength was never large enough to produce an observable pulse. Thus we have seen a new Raman component, in isolation, and observed its effect on the pump.

Early interpretations of the pump depletion process[1],[2] state that the Raman pulse grows as it walks through the pump pulse and attains a maximum when it reaches the leading edge of the pump. Furthermore, because the pump pulse is chirped, the leading red components will be preferentially eaten away. The 1.082 μm pulse; however, presents a seemingly anomalous situation. The Nd:YAG spectrum in this case (Fig. 3B on left) shows the blue, or lagging end to be preferentially depleted. This suggests that due to its lesser walk off velocity, the Raman pulse is saturated before completing its walk through the pump pulse.

A variety of parameters such as throughput power, fiber winding, bending and length strongly affected the fiber output. These effects will be discussed in detail.

Stimulated Raman Scattering

Neil Gitkind, Alfred P. DeFonzo

(1) A.M. Weiner, J.P. Heritage and R.H. Stolen, CLEO'86 Technical Digest, p. 246.

(2) Dieter Schadt, Bozena Jaskorzynska and Ulf Osterberg, to be published.

(3) R.H. Stolen and A.M. Johnson, JQE (1986), to be published.

Stimulated Raman Scattering

Neil Gitkind, Alfred P. DeFonzo

Fig. 1. Spectral and time domain traces of 1.06 μm pulse after propagation through 50 m of single mode fiber. (A) Output pulse measured with a fast photodiode and sampling oscilloscope (47 psec system risetime). 100 psec per division. (B) Spectrum of output pulse. Origin of horizontal scale is the wavelength of incident 1.06 μm pulse.

Fig. 2. Walkoff of 1.12 μm Raman pulse and corresponding spectra after propagation through 400 m of single mode fiber. (A) Exiting Raman pulse at left, Nd:YAG pulse at right. 100 psec per division. (B) Exiting Nd:YAG spectrum (C) 1.12 μm Raman pulse spectrum. Origin of scale is 1.12 μm.

Fig. 3. Walkoff of 1.082 μm Raman pulse and corresponding spectra after propagation through 400 m of single mode fiber. (A) Raman pulse at left, Nd:YAG pulse at right. 100 psec per division. (B) spectra of Nd:YAG pulse at left and 1.082 μm pulse at right. Scale origin is the wavelength of incident 1.06 μm pulse.

(A)

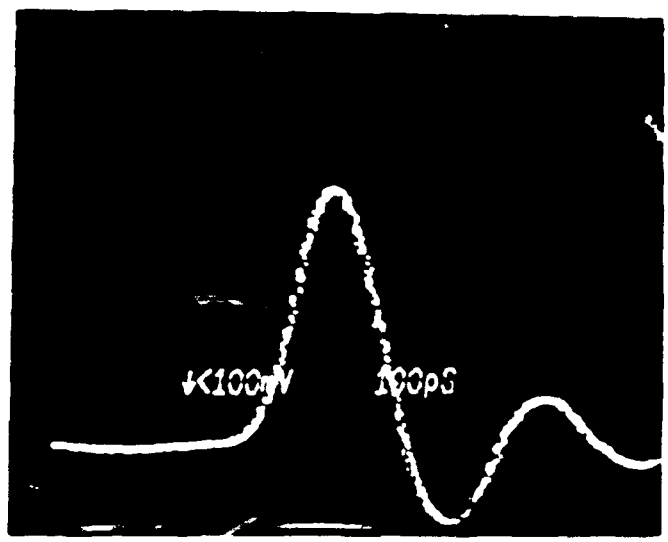

(B)

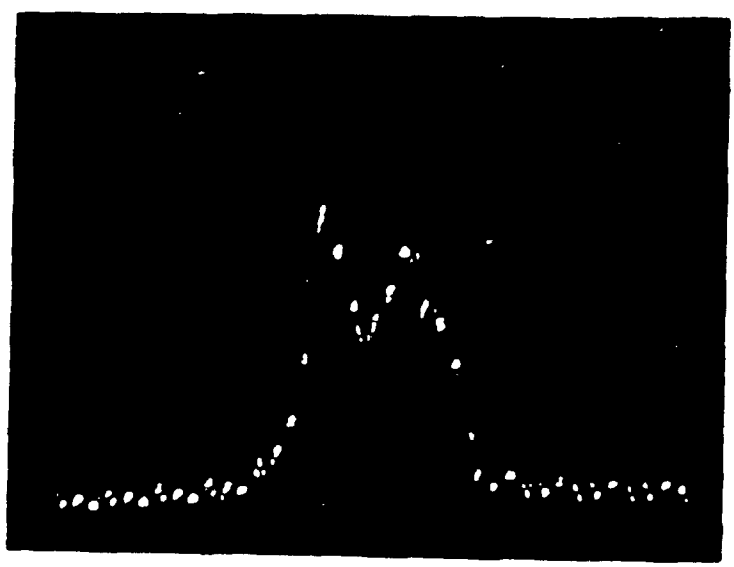

(A)

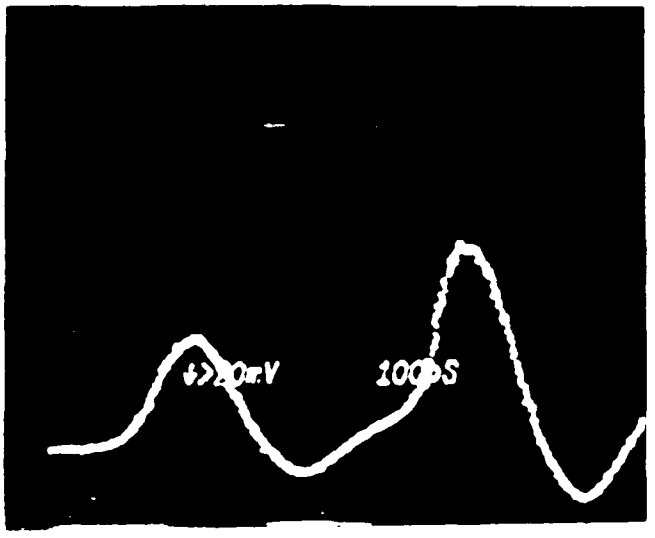

(B)

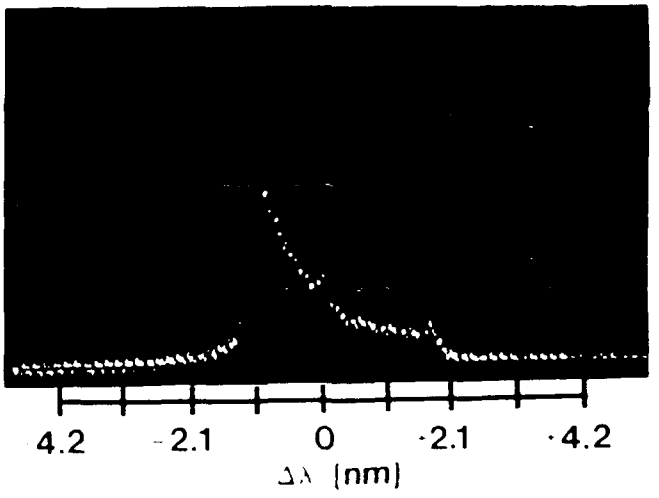

(C)

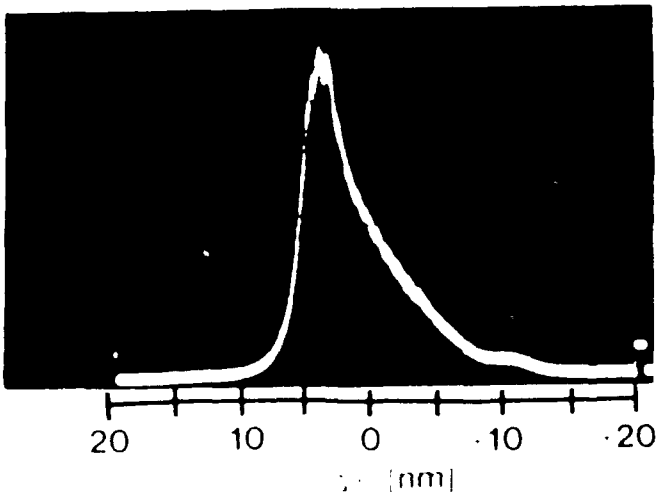

(A)

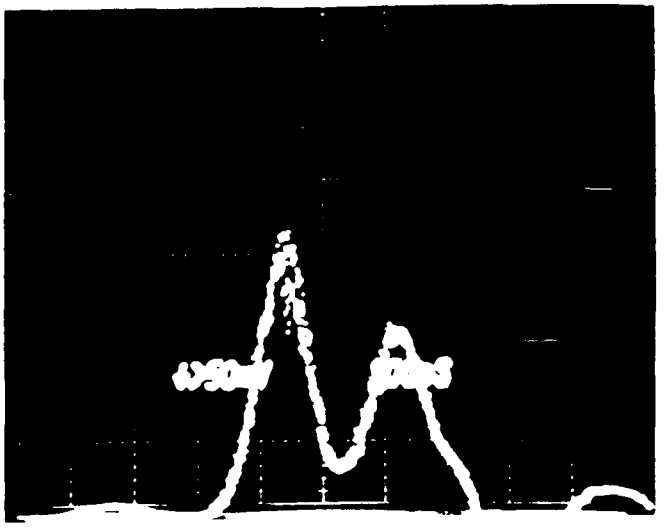

(B)

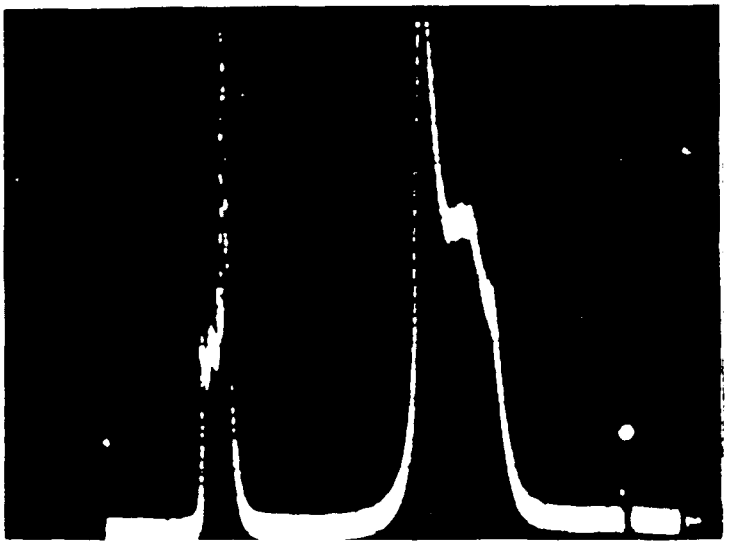

Delete ~~Submitted to~~ Accepted CLEO 87, Nov 17, 1986

Optical Bistability In Single Mode Fibers

ALfred P. De Fonzo and Neil Gitkind
Department of Electrical and Computer Engineering
University of Massachusetts, Amherst MA 01003
413-545-2374

ABSTRACT: We discovered and investigated optical bistability in single mode telecommunication fibers excited by circularly polarized 90 picosecond pulses at 1.06 microns.

We report the first observation of optical bistability in the transmitted power of a single mode optical fiber. The bistabilty occurs when the fiber is pumped with intense modelocked pump pulses at 1.06 microns . The switching of the output occurs near the threshold for Stimulated Raman Scattering and is accompanied by a discontinuous jump in the exiting SRS out and in the magnitude of the pump pulse frequency chirp. Slow scanning of the pump power in the vicinity of the bistability results in large area hysteresis loops. Systematic investigations indicate the presence of a mechanism that produces discontinuous changes in the optical intensity and index of refraction reminiscent of transient self focusing.

The experimental set up, similar to one used in the study of SRS [1], is schematically depicted in Figure 1. Linearly polarized pulses at 1.06 microns are converted to circularly polarized light and coupled into a standard telecommunications fiber (OWEN CORNING 1521). At low powers the circularly polarized light exiting the fiber is converted into linearly polarized light and passed through a Glan Thompson prism with an escape window to allow monitoring of optically induced changes in the state of polarization. The total transmitted pulse power is monitored by both a slow germanium diode and further resolved in time with a high speed InGaAs photodetector (risetime = 35

picoseconds). The output pulses are then spectrally resolved with a grating spectrometer (ISA HR-8) and recorded with a photodiode array. The remaining output beam is also further spectrally resolved with a diffraction grating pair in Littrow configuration and the power at 1.06 microns monitored with a slow silicon diode.

The output power of the pump pulse is plotted as a function of the total output intensity in Figure 2. The dotted line indicates the general form of earlier experiments performed on polarization preserving fiber[2] . At an input power of approximately 2.o watts the output power of the pump suddenly decrease. The dashed lines show the results of slow scanning the critical region. A large hysteresis loop is observed. Further investigating the effect, we found a corresponding sudden increase in the SRS output and the Magnitude of the chirp about 1.06 microns as shown in Figure 3.

The general results are summarized in terms of a model [3] of the optically induced index change in the fiber. The accumulated index change can be determined from a rate analysis and for a gaussian pump pulse has the form:

$$\Delta n(\zeta) = \frac{1}{\tau_1}\int_{-\infty}^{\zeta} \Delta n_0\left(|E(\eta)|^2\right)\exp\left[\frac{-[\zeta-\eta]}{\tau}\right]d\eta$$

Where $\Delta n_0(|E(\eta)|^2)$ is the driving term and E is the optical field for a gaussian pulse. When the total index change =4.37x10^-4 the crossectional area of the pump pulse suddenly decreases, resulting in a further abrupt change in index, that in turn results in increased SRS , chirp production and optical feedback . The critical index change corresponds to the critical power for self focusing in bulk SiO2. We are presently investigating these surprising effects.

REFERENCES

1. Neil Gitkind and Alfred P. De Fonzo, OFC/100C'87
accepted for publication

2. J. Heritage, A.M. Weiner and R.N. Thompson , Proceedings of the Topical Meeting on Ultrafast Phenomenae, Aspen '86

3. A.P. De Fonzo and N. Gitkind -Optics Lettrs. , submitted for publication

FIGURE CAPTIONS

Figure 1. Schematic of Experimental Set Up.

Figure 2. Pump power out versus total (pump + raman) power out for 300 meter single mode fiber. Solid and dashed lines our data. Dotted line shows from of data reported for polarization preserving fiber [2].

Figure 3. Chirp of the pump pulse and the Raman power output as a function of the total input pump power in a 300 meter long single mode fiber.

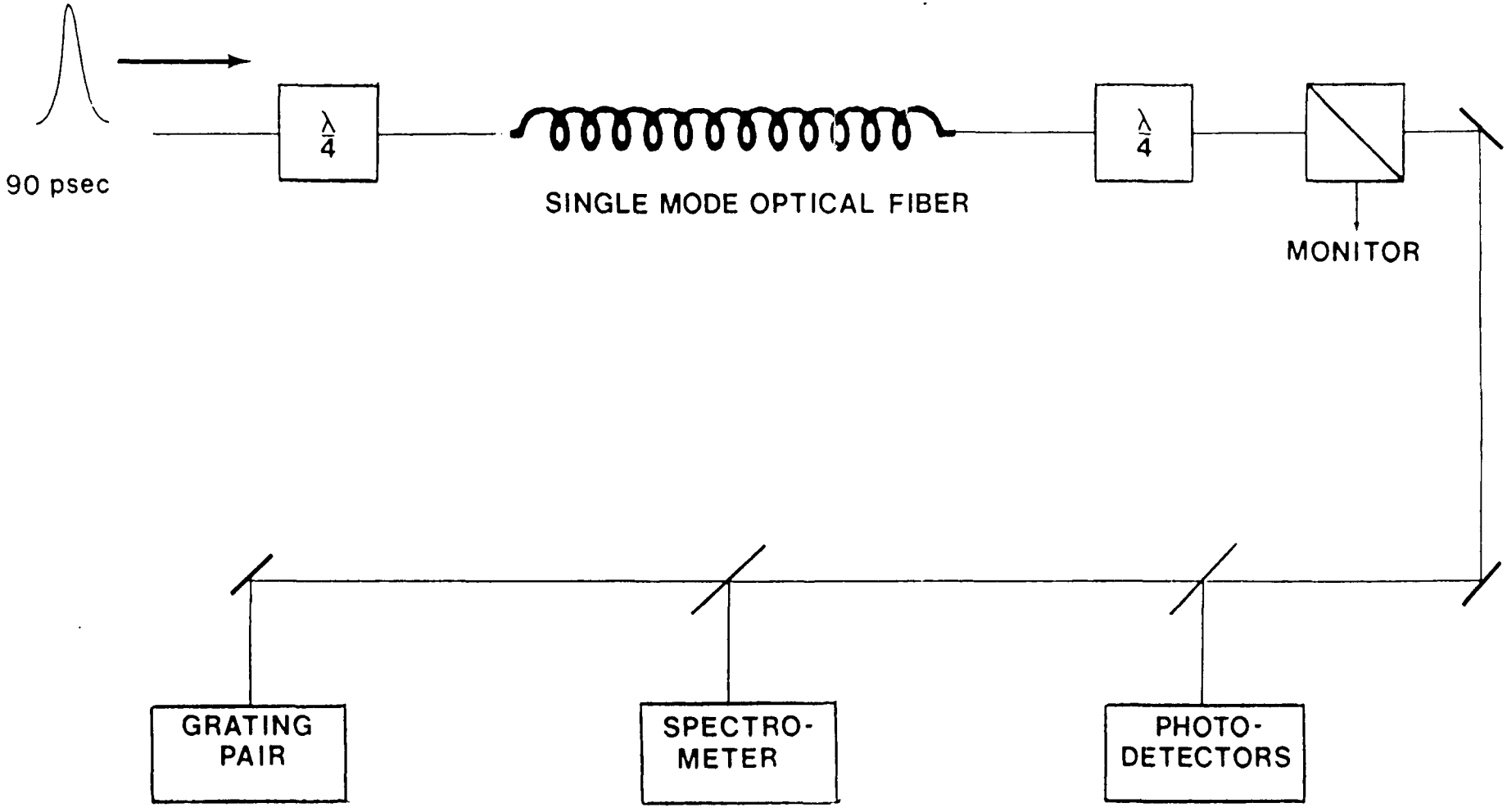
90 psec
λ/4
SINGLE MODE OPTICAL FIBER
λ/4
MONITOR
GRATING PAIR
SPECTRO-METER
PHOTO-DETECTORS

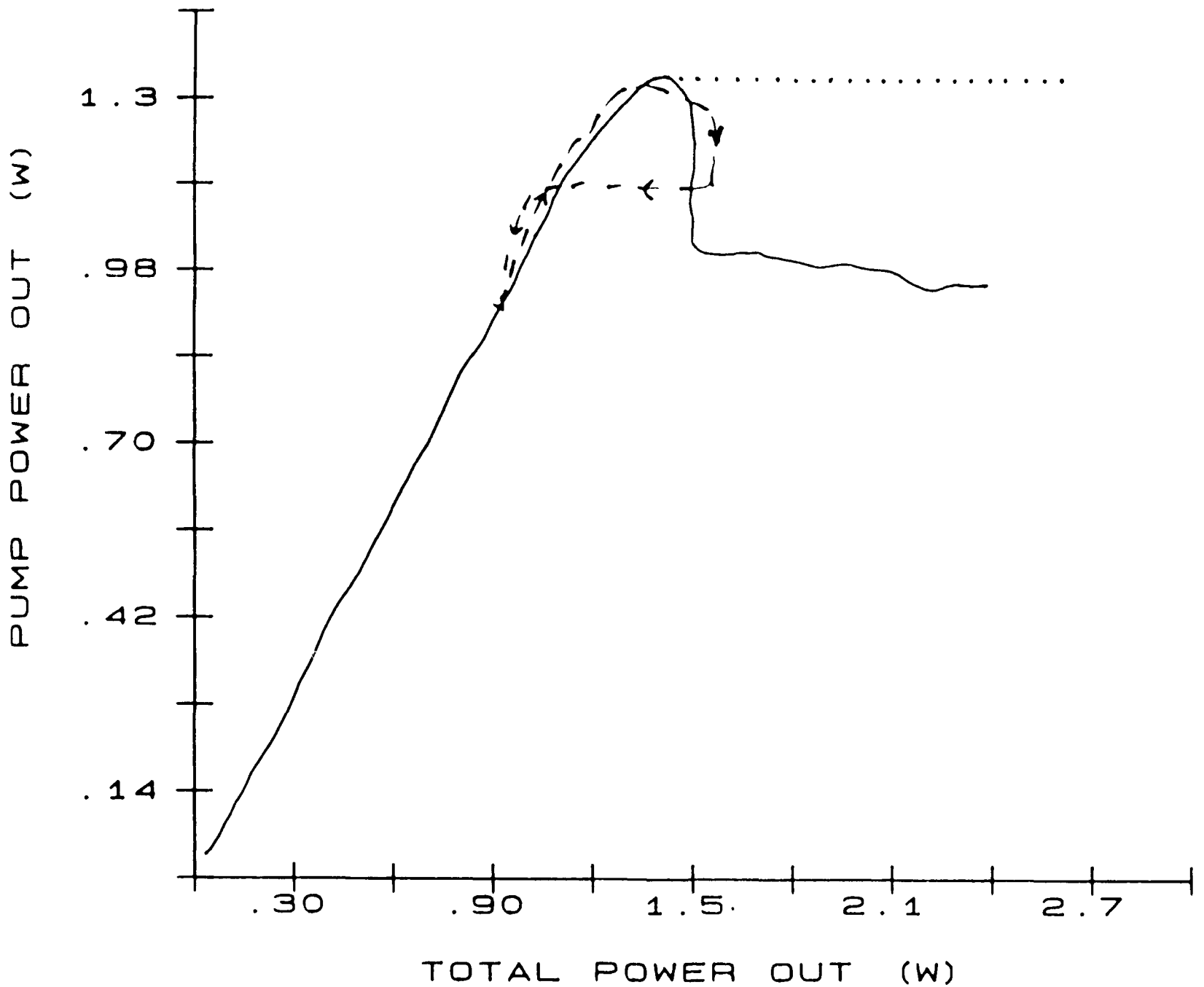
1.3
.98
.70
.42
.14
PUMP POWER OUT (W)
.30
.90
1.5
2.1
2.7
TOTAL POWER OUT (W)

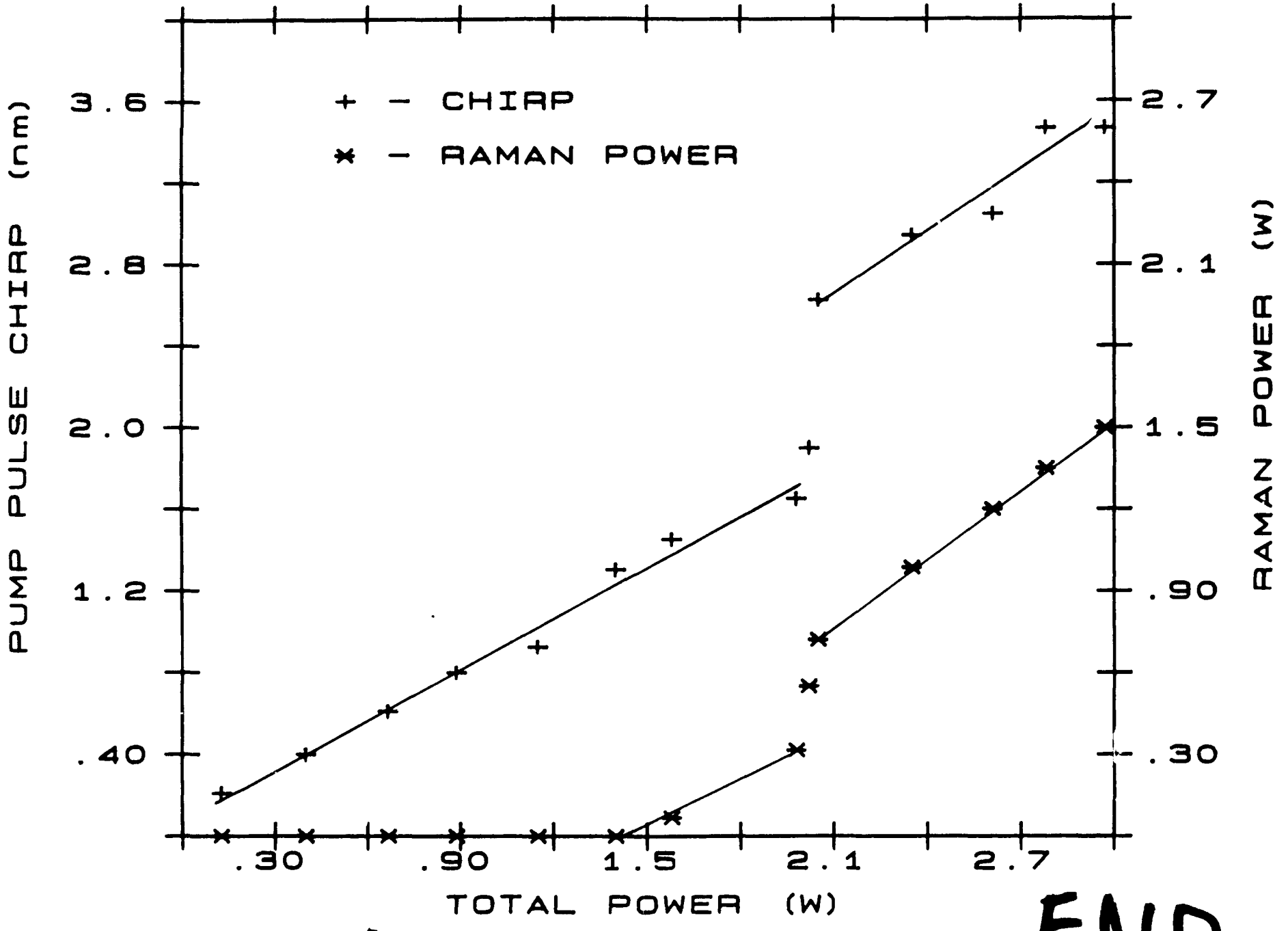
+ - CHIRP
* - RAMAN POWER
PUMP PULSE CHIRP (nm)
RAMAN POWER (W)
TOTAL POWER (W)
3.6
2.8
2.0
1.2
.40
2.7
2.1
1.5
.90
.30
.30
.90
1.5
2.1
2.7

END